Biochemical Pharmacology 192 (2021) 114688

Contents lists available at ScienceDirect

Biochemical Pharmacology

journal homepage: www.elsevier.com/locate/biochempharm

TTI-101: A competitive inhibitor of STAT3 that spares oxidative phosphorylation and reverses mechanical allodynia in mouse models of neuropathic pain

Moses M. Kasembeli [a], Pooja Singhmar [b], Jiacheng Ma [b], Jules Edralin [b], Yongfu Tang [b], Clydell Adams III [a], Cobi J. Heijnen [b], Annemieke Kavelaars [b], David J. Tweardy [a,*]

[a] The Department of Infectious Diseases, Infection Control & Employee Health and the Department of Symptom Research, 1400 Pressler Street, FCT12.5069, Unit 1463, Houston, TX 77030-3772, United States

[b] Division of Internal Medicine, University of Texas MD Anderson Cancer Center, 1515 Holcombe Boulevard, Houston, TX 77030-4009, United States

ARTICLE INFO

Keywords:
STAT3
neuropathic pain
allodynia
CIPN
TTI-101
VEGF

ABSTRACT

Signal Transducer and Activator of Transcription (STAT) 3 emerged rapidly as a high-value target for treatment of cancer. However, small-molecule STAT3 inhibitors have been slow to enter the clinic due, in part, to serious adverse events (SAE), including lactic acidosis and peripheral neuropathy, which have been attributed to inhibition of STAT3′s mitochondrial function. Our group developed TTI-101, a competitive inhibitor of STAT3 that targets the receptor pY705-peptide binding site within the Src homology 2 (SH2) domain to block its recruitment and activation. TTI-101 has shown target engagement, no toxicity, and evidence of clinical benefit in a Phase I study in patients with solid tumors. Here we report that TTI-101 did not affect mitochondrial function, nor did it cause STAT3 aggregation, chemically modify STAT3 or cause neuropathic pain. Instead, TTI-101 unexpectedly suppressed neuropathic pain induced by chemotherapy or in a spared nerve injury model. Thus, in addition to its direct anti-tumor effect, TTI-101 may be of benefit when administered to cancer patients at risk of developing chemotherapy-induced peripheral neuropathy (CIPN).

1. Introduction

STAT3 is known to play an essential role in biological processes important for development, including cell growth and survival, as well as in restoring homeostasis after injury. However, persistent STAT3 signaling has been linked to a number of pathological conditions including cancer, chronic inflammation and fibrosis. An extensive body of preclinical data indicates that inhibition of STAT3 signaling may be of substantial therapeutic benefit [1,2]. However, agents that target STAT3 have been slow to enter the clinic, in part, because of difficulties inherent in targeting transcription factors, a class of proteins deemed “undruggable” due to the large size of their protein–protein interaction interfaces [3]. In addition, serious adverse events (SAE), including lactic acidosis and peripheral neuropathy, have been observed with some small-molecule STAT3 inhibitors in clinical-stage development [4,5]. These have been attributed to targeting of STAT3’s non-canonical functions, most notably, its contribution to mitochondrial-mediated oxidative phosphorylation [6], which relies on phosphorylation of STAT3 on serine 727, in contrast to phosphorylation on tyrosine 705 required for its canonical function [7,8].

Many STAT3-directed drug development programs have focused on STAT3′s SH2 domain, in particular its phosphotyrosine (pY) peptide binding pocket. However, the finding that some inhibitors induce mitochondrial toxicity suggests they may target other regions of STAT3 and affect STAT3 structure and stability. In fact, Genini et al. demonstrated that OPB-51602, and other small-molecule STAT3 inhibitors designed to directly target STAT3, caused STAT3 aggregation and altered intracellular protein homeostasis [6]. They further argued that induction of cell death by these agents is mediated, in part, through a proteotoxic mechanism in metabolically stressed cancer cells and suggested that this may be a common mechanism underlying the anticancer activity of any inhibitor that directly targets the SH2 domain within STAT3.

Our group, working in collaboration with Tvardi Therapeutics, Inc., developed TTI-101 (formerly C188-9), a competitive inhibitor of STAT3 designed to target the pY-peptide binding site within STAT3′s SH2

* Corresponding author.
E-mail address: djtweardy@mdanderson.org (D.J. Tweardy).

https://doi.org/10.1016/j.bcp.2021.114688
Received 3 May 2021; Received in revised form 11 July 2021; Accepted 13 July 2021
Available online 16 July 2021
0006-2952/© 2021 The Author(s). Published by Elsevier Inc. This is an open access article under the CC BY-NC-ND license (http://creativecommons.org/licenses/by-nc-nd/4.0/).

domain and thereby directly block two key steps in its activation—recruitment to activated cytokine receptor complexes and homodimerization [9,10]. We previously performed good laboratory practice (GLP)-compliant, 28-day pharmacotoxicology studies of TTI-101 [10] that demonstrated no drug-related toxicity up to the maximum dose administered (200 mg/kg/day in rats and 100 mg/kg/day in dogs). Moreover, an ongoing Phase I clinical trial of TTI-101 that has enrolled 40 patients with advanced solid tumors [11] up to dose level 4 (25.6 mg/kg/day) for as long as 12 months, has not demonstrated any serious adverse events, including lactic acidosis.

The studies reported here were undertaken to determine *in vitro* if TTI-101 affects STAT3 mitochondrial function, causes STAT3 aggregation, chemically modifies STAT3, or induces peripheral neuropathy in mice. We tested TTI-101 and four other STAT3 inhibitors purported to target the STAT3 SH2 domain and demonstrated that two of these—WP-1066 and cryptotanshinone—induced STAT3 aggregation and caused mitochondrial toxicity in metabolically stressed cells. Importantly, our studies revealed that TTI-101 does not: 1) affect mitochondrial function, 2) chemically modify STAT3, 3) cause STAT3 aggregation in metabolically stressed cells, or 4) cause peripheral neuropathy. In fact, TTI-101 administration unexpectedly reversed mechanical allodynia in models of chemotherapy-induced peripheral neuropathy (CIPN) and spared nerve injury (SNI). These findings indicate that TTI-101 may be of special benefit when administered to patients receiving CIPN-inducing agents as part of their cancer therapy regimen.

2. Material and methods

2.1. Materials

STAT3 inhibitors - Stattic, cryptotanshinone, WP1066 and STA21 were obtained from Selleck Chemicals (Houston, TX, USA). TTI-101 was custom synthesized by Regis technologies Inc. (Morton Grove, IL, USA). Molecular grade dimethyl sulfoxide (DMSO), reduced glutathione (GSH), iodoacetamide, and N-ethylmaleimide were obtained from Sigma-Aldrich (St. Louis, MO, USA). Cisplatin was acquired from (TEVA Pharmaceuticals, North Wales, PA). All LC/MS reagents, including ammonium acetate, formic acid, acetonitrile, methanol and water, were obtained from Honeywell Fluka (Morris Plains, NJ, USA). STAT3 antibody was purchased from Cell Signaling Technology (Danvers, MA, USA). Antibodies to histone H2B (ab52484) and GAPDH (ab9485) were purchased from Abcam (Toronto, ON, Canada). Antibody to Vimentin (sc66002) was obtained from Santa Cruz Biotechnology (Dallas, TX, USA). DMEM XF base medium, FCCP, and rotenone/antimycin A were obtained from Agilent Technologies (Santa Clara, CA, USA). A C18 Synergi™ 4 μm Fusion-RP 80 Å LC column (50 × 2 mm) was purchased from Phenomenex, (Torrance, CA, USA); a Waters Symmetry C18 column (100 Å, 3.5 μm, 4.6 mm × 150 mm) was purchased from Waters (Milford, MA, USA).

2.2. Cell line and culture

The human prostate cancer cell line DU-145 was obtained from American Type Culture Collection (ATCC, Rockville, MD, USA) and cultured in RPMI 1640 medium (ATCC modification) containing 10% fetal bovine serum and Antibiotic-Antimycotic from Gibco, Invitrogen (Carlsbad, CA, USA). The cells were cultured at 37 °C with an atmosphere of 5% CO_2.

2.3. Mitochondrial assays

DU-145 cells (2.5×10^4) were seeded per well in XF24 plates and incubated at 37 °C / 5% CO_2 in complete RPMI medium. After 12Hrs complete medium was replaced with nutrient depleted four-day culture media: conditioned media (CM) and incubated for 4 Hrs. Cells were then treated for another 2 Hrs with STAT3 inhibitors prior to analysis using a Seahorse XF24 Analyzer. The Oxygen Consumption Rate (OCR) was measured in DMEM XF base medium containing 10 mM glucose, 2 mM glutamine and 1 mM pyruvate, before and after the sequential injection of oligomycin, FCCP and rotenone/antimycin A, as indicated in (Fig. 1), to final concentrations of 1 uM, 1 uM and 0.5 uM, respectively.

2.4. Cell fractionation

Cells were treated for 16 Hrs with STAT3 inhibitors at a concentration of 10 uM and 1% DMSO in glucose depleted conditioned media (CM), as described [6]. Lysates were fractionated into cytosol, organelle, nuclei, and cytoskeleton subcellular fractions using ProteoExtract kit (Calbiochem, San Diego, California, USA) according to the manufacturer's directions. Enrichment of each fraction was assessed by SDS-PAGE and immunoblotting using antibodies against GAPDH (cytosol and organelles, Fractions I and II), Histone H2B (nucleus, Fraction III), and Vimentin (cytoskeleton and insoluble proteins, Fraction IV).

2.5. Expression and purification of recombinant STAT3

STAT3 (127–722) cDNA was cloned into a pET15b vector and transformed in BL21 (DE) (Life Technologies, Inc. Woburn, MA, USA). Expression of the recombinant protein was induced by 0.5 mM IPTG, at 20 °C for 5 Hrs. The recombinant STAT3 protein was purified by ammonium sulfate precipitation followed by an ion exchange step with a HiTrap Q column (GE Healthcare Bio-Sciences, Uppsala Sweden) and size exclusion chromatography to achieve purity of over 98%.

2.6. Glutathione reaction studies

STAT3 inhibitors (10 ul of 10 mM stock in DMSO) were spiked into reaction buffer [50 mM HEPES pH7.5 containing 10 mM reduced glutathione (GSH)] the samples were mixed thoroughly and placed in an autosampler set at 20 °C. The reactions were monitored by high performance liquid chromatography (HPLC) using an Exion LC Sciex unit equipped with a UV detector. The stationary phase used was a C18 Synergi™ 4 μm Fusion-RP 80 Å LC column (50 × 2 mm), the mobile phase was water (A) and acetonitrile (B). The elution process consisted of a gradient starting at 20% mobile phase B to 80% for 2 min. The flow rate was maintained at 0.5 mL/min during the run. Measurements were conducted at intervals of 5 min for a period of 50 min total. The presence of the STAT3 inhibitors were quantified by calculating the area under the curves (AUCs) of the compound peaks at 260–295 nm.

2.7. STAT3 alkylation studies

Purified recombinant core fragment of STAT3β protein in ammonium bicarbonate buffer (10 uM) was mixed with each compound at a final concentration of 100 uM. The protein mixture was then incubated at 37 °C overnight. Samples were reduced with 5 mM DTT at 37 °C for one hour and further alkylated with iodoacetamide (15 mM) for 30 min at room temperature in the dark, followed by digestion with trypsin gold in a dry incubator at 37 °C overnight. Formic acid was added the next day to a final concentration of 5% and each protein sample was diluted in 5 mM ammonium acetate containing 0.5% formic acid immediately prior to analysis by targeted mass spectrometry Multiple Reaction Monitoring (MRM).

2.8. Lc–MS/MS

A QTRAP 5500 Sciex hybrid quadrupole-linear ion trap system with a turbo ion spray source coupled to a Sciex LC Exion liquid chromatography system (Redwood City, CA, USA) were used to analyze tryptic digests of STAT3 protein samples treated with STAT3 inhibitors. Fractionation of the samples was done using a Waters Symmetry C18 column (100 Å, 3.5 μm, 4.6 mm × 150 mm) with a 30 min linear gradient of

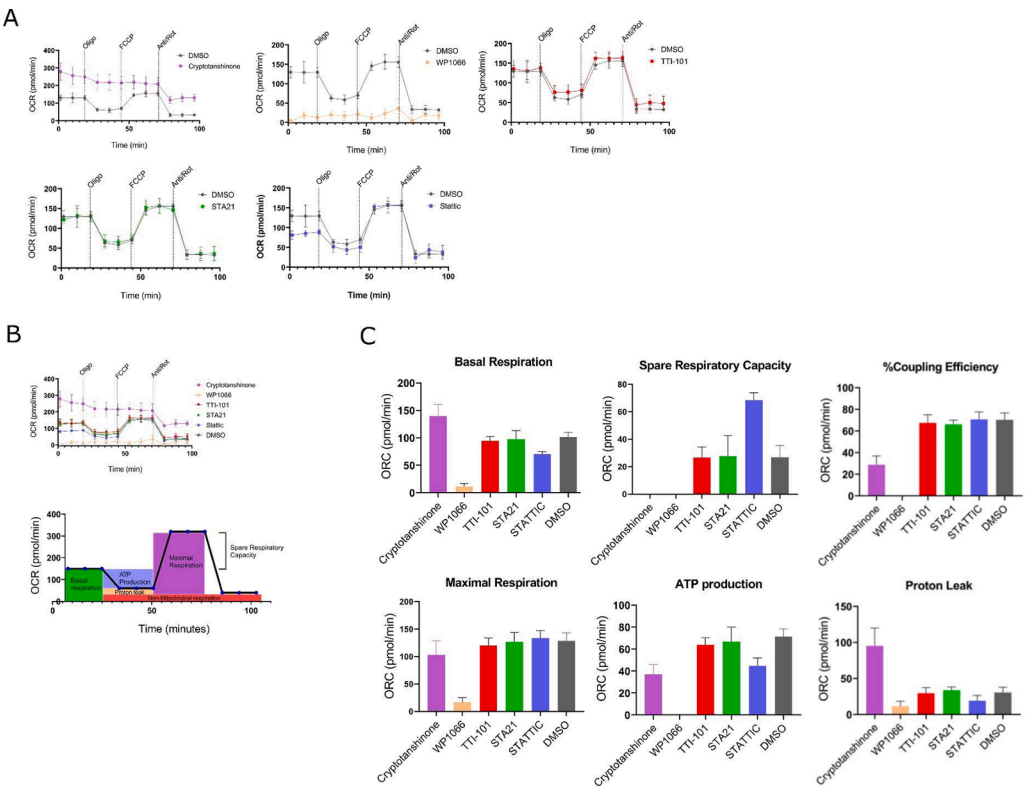

Fig. 1. Effects of STAT3 inhibitors on mitochondrial function. DU-145 cells were treated with the indicated STAT3 inhibitors at 30 uM for 2 Hrs. Seahorse experiments showing oxygen consumption rate (OCR) by DU-145 cells treated with DMSO alone or DMSO containing the indicated STAT3 inhibitor at 30uM prior to and following addition of oligomycin, FCCP, and antimycin A/rotenone, as indicated (n = 6). Data in (Fig. 1 A) combined into one graph, showing all the OCR curves relative to each other. Below, figure representing estimation of OCR parameters in(C) Mean ± SEM of basal respiration, maximal respiration, spare respiratory capacity, ATP production, coupling efficiency and proton leak (n = 6).

acetonitrile containing 0.1% formic acid at a flow rate of 300 uL/min. A transition list of cysteine-containing peptides with expected drug-cysteine adducts was generated in Skyline software and exported to the QTRAP mass spectrometer for the development of the acquisition method. Resultant raw data files were imported back into Skyline for analysis and additional processing.

2.9. High resolution LC/MS

Aliquots of the tryptic digests of STAT3 proteins treated with DMSO (control) and those treated with Stattic and TTI-101 were analyzed by LC-MS/MS on an Ultimate 3000 RSLC-Nano chromatograph interfaced to an Orbitrap Fusion high-resolution mass spectrometer (Thermo Scientific, Waltham MA). All MS/MS data were analyzed using Sequest-HT (Thermo Scientific). Proteins were identified by searching their fragment spectra against the Swiss-Prot protein database (EBI). The iodoacetamide derivative of cysteine, stattic adducts of cysteine, and the predicted TTI-101 adducts of cysteine were specified as variable modifications. To access for potential unknown modifications, the data was analyzed in MaxQuant using the dependent peptide search option [12]. An all-peptides output list was analyzed by comparing Stattic, TTI-101 and TTI-101$_{ox}$ with DMSO treated samples, as described in [13].

2.10. Animals

Male and female C57BL/6J mice were purchased from Jackson Laboratories (Bar Harbor, ME) and housed at the University of Texas MD Anderson Cancer Center animal facility (Houston, TX) on a regular 12-hour light/dark cycle with free access to food and water. Mice were group-housed on the same rack in individually ventilated cages. Mice were 8 – 10 weeks of age at the start of the experiment and were randomly assigned to groups (cage) by animal care givers not involved in the experiment. Investigators were blinded to treatment until group data were analyzed and the code was broken by an investigator not involved in the study. All experimental procedures were consistent with the National Institute of Health Guidelines for the Care and Use of Laboratory Animals and the Ethical Issues of the International Association for the Study of Pain [14] and were approved by the Institution for Animal Care and Use Committee (IACUC) of M.D. Anderson Cancer Center. Experiments were performed and reported in compliance with the ARRIVE guidelines [15].

2.11. Pain measurements and chemotherapy-induced peripheral neuropathy (CIPN)

The effect of TTI-101 and chemotherapy on mechanical sensitivity as a read out for pain were assessed over time using von Frey hairs (0.02, 0.07, 0.16, 0.4, 0.6, 1.0, and 1.4 g; Stoelting, (Wood Dale, Illinois, USA) and the up and down method as described previously [16,17]. Cisplatin was diluted in sterile PBS and administered i.p. at a dose of 2.3 mg/kg per day for 5 days followed by 5 days of rest and another 5 days of injections [18]. After 17 days of the last dose of cisplatin the mice were treated with TTI-101 (50 mg/kg i.p. every other day) for a total of seven doses.

2.12. Spared nerve injury (SNI)

SNI surgery was performed on male and female C57BL/6j mice (8 weeks old; Jackson Laboratories), as described [19]. The sural, common peroneal and tibial branches of the sciatic nerve of the left hind paw were exposed under isoflurane anesthesia. A silk suture was used to ligate the common peroneal and tibial branches and 2–4 mm of the distal ends were removed. The sural nerve was left intact. Mice received buprenorphine right before and 1 h after surgery. Mice were treated with 6 doses of TTI-101 (50 mg/kg in vehicle—60% Labrasol/40% PEG-400—or vehicle alone) administered by oral gavage every other day starting on day 10 after SNI. Mechanical sensitivity was monitored over time using von Frey hairs.

2.13. Data and analysis

Studies were designed to include groups of equal size, using randomization and blinded analysis. Statistical analysis was undertaken for studies where each group size was at least n = 5, with the exception of the CIPN study where 4 mice per group were used. Animal group size selection for mechanical allodynia was based on previously published data for similar experiments in which sample size calculations were established [19]. Pain behavior data were normally distributed and analyzed by Two-way repeated measures ANOVA followed by Tukey post tests using PRISM8 software; $P < 0.05$ was considered statistically significant. Data from all animals enrolled were included in the final analysis.

2.14. RNA-seq and transcriptome analysis of dorsal root ganglion (DRG)

Whole-genome RNA sequencing was used to identify transcriptional changes induced by cisplatin and TTI-101 in the DRG of 3 mice per group. Total RNA was isolated with the RNeasy MinElute Cleanup Kit (Qiagen, Hilden, Germany). Libraries were prepared with the Stranded mRNA-Seq kit (Kapa Biosystems, Wilmington, MA) following the manufacturer's guidelines. Stranded-mRNA seq was performed with a HiSeq4000 Sequencer (Illumina, San Diego, CA) with 76nt PE format by the RNA Sequencing Core at MD Anderson Cancer Center.

Data analysis was performed as previously described [20,21]. Briefly, expression data of three samples per group were analyzed in R using bioconductor packages. STAR was used for alignment of paired-end reads to the mm10 version of the mouse reference genome; featureCounts was used to assign mapped sequence reads to genomic features, and DESeq2 was used to identify differentially expressed genes (padj < 0.05). Quality check of raw and aligned reads was performed with FastQC and Qualimap. Next, we used Ingenuity Pathway Analysis (IPA;Qiagen Inc., https://www.qiagenbioinformatics.com/products/ingenuity-pathway-analysis/) for analysis of the canonical pathways implicated by cisplatin-induced transcriptome changes in DRG.

3. Results

3.1. TTI-101 does not affect mitochondrial function

Mitochondrial dysfunction has been demonstrated to contribute to drug-related SEA [22]. Examination of TTI-101 for safety in 28-day IND-enabling studies in rats and dogs [9], as well as in a Phase I clinical trial of patients with advanced solid tumors through dose level 4 [11], did not demonstrate any serious toxicity including lactic acidosis, which is a clinical manifestation of mitochondrial dysfunction. However, to determine if TTI-101 caused subclinical abnormalities in mitochondrial function, we examined the effects of TTI-101 and four other direct STAT3 inhibitors on mitochondrial respiration using a Seahorse XF Cell Mito Stress Test kit that measured basal respiration, ATP production, maximal respiration, proton leak, and spare respiratory capacity. The OCR curves of cells incubated with TTI-101 at concentrations 10-fold higher than its IC_{50} for STAT3 inhibition [9] were similar to cells treated with DMSO control **(**Fig. 1**A-C)**. Similarly, STA21 and Stattic did not consistently alter the OCR curves compared to DMSO at these concentrations **(**Fig. 1**A-C)**.

In contrast, marked abnormalities were observed in the OCR curves of cells treated with cryptotanshinone and WP1066 (Fig. 1**A, B)**. Overall, the effects of cryptotanshinone on the OCR curves mimicked a mitochondrial uncoupler, which creates a 'shot-circuit' in the oxidative process by inducing a proton leak (PL) such that the loss of proton motive force proceeds without ATP generation. Cells incubated with cryptotanshinone (30 uM) demonstrated a concentration-dependent increase in basal respiratory rate compared to control cells and decreased responses to oligomycin and to antimycin A/rotenone treatment. In addition, cryptotanshinone blocked cell responses to FCCP treatment and resulted in a 50% reduction in ATP level production. **(**Fig. 1**A-C)**. To further examine the effects of cryptotanshinone on ATP production, we measured the fraction of basal mitochondrial oxygen consumption linked to ATP synthesis (coupling efficiency); coupling efficiency was significantly reduced **(**Fig. 1**C)**, further indicative of mitochondrial dysfunction. In addition, the OCR after oligomycin treatment, which is a direct measure of the proton leak rate **(**Fig. 1**C)**, showed a significant increase in proton leak in cells incubated with cryptotanshinone (30 uM) indicating that mitochondria are uncoupled and severely damaged [23,24]. Similar to cryptotanshinone, we observed marked abnormalities in the OCR curves of cells treated with WP1066. (Fig. 1**A-C**) indicative of mitochondrial dysfunction [24], including diminished basal OCR, ATP production rate, maximal respiration, spare respiratory capacity, and coupling efficiency.

3.2. TTI-101 does not induce STAT3 aggregation in cells

STAT3 inhibitors that were demonstrated to impair mitochondrial activity also were found to cause STAT3 to aggregate in cells under low glucose conditions [6]. Using similar experimental conditions, we assessed the effects of TTI-101 and other direct STAT3 inhibitors on the partitioning and oligomeric state of STAT3. Cells were incubated in medium containing each STAT3 inhibitor at 10 uM final concentration for 16 h. Cells were fractionated and fractions I through IV were separated by SDS-PAGE and immunoblotted using antibodies selective for each fraction (Fig. 2). TTI-101 had no effect on the intracellular localization of STAT3; similar results were obtained in cells incubated with STA21 and Stattic. In contrast, in cells treated with cryptotanshinone or WP1066, over half of STAT3 was found in the insoluble fraction (Fraction IV) indicating that each induced formation of STAT3 intracellular aggregates, which explains their adverse effects on mitochondrial function and confirms the findings of Genini et.al. [6].

3.3. TTI-101 does not react with GSH or covalently modify STAT3

Surface Plasmon Resonance (SPR) studies that directly examined the ability of TTI-101 to inhibit STAT3 binding to its immobilized pY-peptide ligand were performed under reducing conditions [9,25]. Furthermore, the shape of the binding inhibition curves was most consistent with competitive inhibition. However, intracellular protein depletion through aggregation has recently been described as a key mechanism of action of compounds, such as DUB Inhibitors b-AP15 and VLX1570 that possess α,β-unsaturated carbonyl moieties capable of covalently reacting with their target [26]. Soon after its discovery, Stattic was proposed to alkylate STAT3 via a Michael addition reaction at C687 located within the SH2 domain, but outside the pY-peptide binding pocket; this alkylation event was proposed to allosterically alter the structure of the pY-peptide binding pocket interfering with its ability to bind ligand [27]. More recently, SI3-201 and related compounds were shown to modify STAT3 in a manner consistent with thiol-mediated *O*-tosyl substitution [28].

We performed two studies to determine directly if TTI-101 mediates its inhibitory effect on STAT3 through covalent modification. The first study was a UV-HPLC-based assay to determine the stability of TTI-101, as well as the other STAT3 inhibitors, in the presence of a natural nucleophile—reduced glutathione (GSH). TTI-101 and the other inhibitors were reconstituted at 100 uM in 50 mM HEPES buffer at pH 7.5 containing 10 mM GSH. Each reaction mixture was sampled at time 0 and every 5 min for 50 min; all samples were analyzed by HPLC. The amount of unreacted inhibitor was determined by measuring the area under the curve (AUC) and plotting this value as a percentage of the starting AUC as a function of time **(**Fig. 3**)**. Consistent with early reports of it serving as a Michael's acceptor, Stattic levels decreased rapidly within 5 min to < 10% of baseline in the presence of GSH while remaining constant in the absence of GSH (Fig. 3). In contrast, there was no loss of TTI-101 in the presence of GSH up to 50 min after exposure;

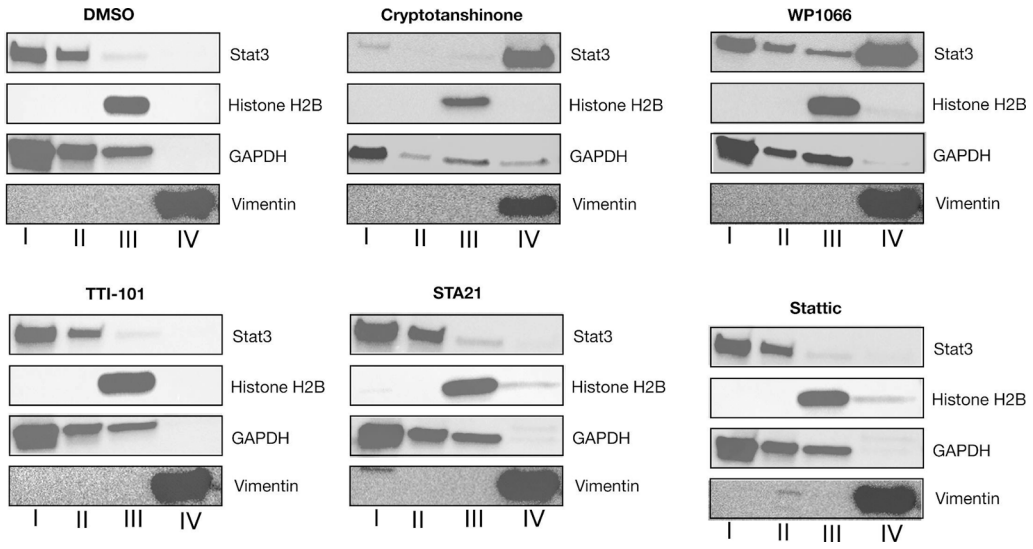

Fig. 2. Immunoblotting of fractions of DU-145 cells incubated with indicated drugs (10uM concentration for 16 Hrs). Fractions were separated using 4–20 % SDS-PAGE and immunoblotted using antibodies against STAT3, Histone H2B, GAPDH and Vimentin. Data are representative of three independently performed experiments.

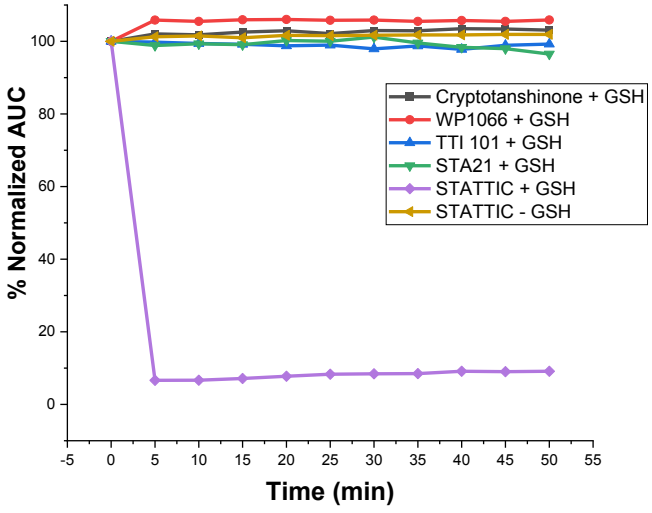

Fig. 3. Stability of compounds incubated with GSH. The AUC of each compound measured at the times indicated by UV-HPLC and expressed as percent of the starting AUC of the peaks. Data are representative of four independently performed experiments.

similar results were observed for cryptotanshinone, WP1066 and STA21.

Review of the structure of TTI-101 did not reveal a potential mechanism for alkylation of STAT3 by a Michael addition or by thiol-mediated *O*-tosyl substitution. However, enol-to-ketone oxidation within the first hydroxy-naphthalene group of TTI-101 would form TTI-101_{OX} (Fig. 4**)**, which potentially could undergo a Michael addition reaction. To examine this possibility, we generated recombinant STAT3 post-translationally unmodified in bacteria using a cDNA construct in which the domain containing the N-terminal oligomerization domain was deleted (STAT3β tr); this domain is not necessary for native folding of the core domains of STAT3 (CCD, DBD, linker domain, and SH2 domain) and its removal markedly improves recombinant STAT3 protein solubility. STAT3β tr contains 11 Cys residues. To determine how many of these Cys residues are available to be alkylated when the soluble protein is natively folded, we incubated STAT3β tr with two protein alkylating agents, iodoacetamide and N-ethylmaleimide (NEM) under conditions optimal for alkylation (Fig. 4**A**). Using data obtained on a quadrupole-linear ion trap MS (Sciex QTrap 5500), we detected adducts based on the presence of predicted MRM signal for peptides containing cysteine residues. The identity of the peptides were confirmed by performing full MS/MS spectra on the detected transitions. The LC-MS/MS of the tryptic digested protein revealed 6 peptides alkylated by iodoacetamide and NEM. Five of the peptides contained a single alkylated Cys, while one of the peptides contained two alkylated Cys residues.

We next performed targeted and untargeted LC-MS/MS analysis using a QTrap 5500 and an Orbitrap-Ellite mass spectrometer on tryptic digests of STAT3β tr incubated with TTI-101 or Stattic under optimal alkylating conditions. If TTI-101 or TTI-101_{OX} alkylated STAT3, we would expect a shift in the mass of peptides containing Cys residues by the equivalent of the exact mass of TTI-101ox as TTI-101 needs to undergo oxidation at the –OH located para to the sulfonamide group to form a Michael's acceptor. We were unable to detect adducts of TTI-101 or TTI-101ox on Cys containing peptides by targeted LC-MS/MS (Fig. 4**C)**. To ensure that the failure to detect alkylated protein incubated with TTI-101 was not due to insufficient generation of oxidized TTI-101 under the experimental conditions, we synthesized TTI-101_{OX} itself and incubated it with STAT3 β tr. Similar to results obtained with TTI-101, no alkylated peptides were detected upon incubation with TTI-101_{OX} indicating that STAT3 is not alkylated by TTI-101 in either its reduced or oxidized form. In contrast to TTI-101, tryptic digests of STAT3β tr incubated with Stattic under similar conditions demonstrated that Stattic efficiently alkylated STAT3 at seven sites (Fig. 5 **A-C)**.

We then evaluated the possibility that TTI-101—reduced or oxidized—may covalently modify STAT3 and result in a mass shift on LC-MS/MS that is not detectable using the targeted detection approach described above. We performed high resolution LC-MS/MS analysis of protein digests after incubation of STAT3 with TTI-101 or TTI-101_{OX} using an Orbitrap-Ellite mass spectrometer and analyzed the data using an approach described by Antinori et. al that is tailored for the detection of unknown chemical adduct modifications on proteins [13]. Using this approach, we were able to detect Stattic adducts in protein digests of STAT3 incubated with Stattic. However, we did not identify adducts in digests of STAT3 incubated with either TTI-101 or TTI-$101_{OX,}$ confirming that neither forms of TTI-101 covalently modify STAT3 (Fig. 5 **D)**.

3.4. TTI-101 suppresses chemotherapy-induced mechanical allodynia

Peripheral neuropathy has been observed with several small-

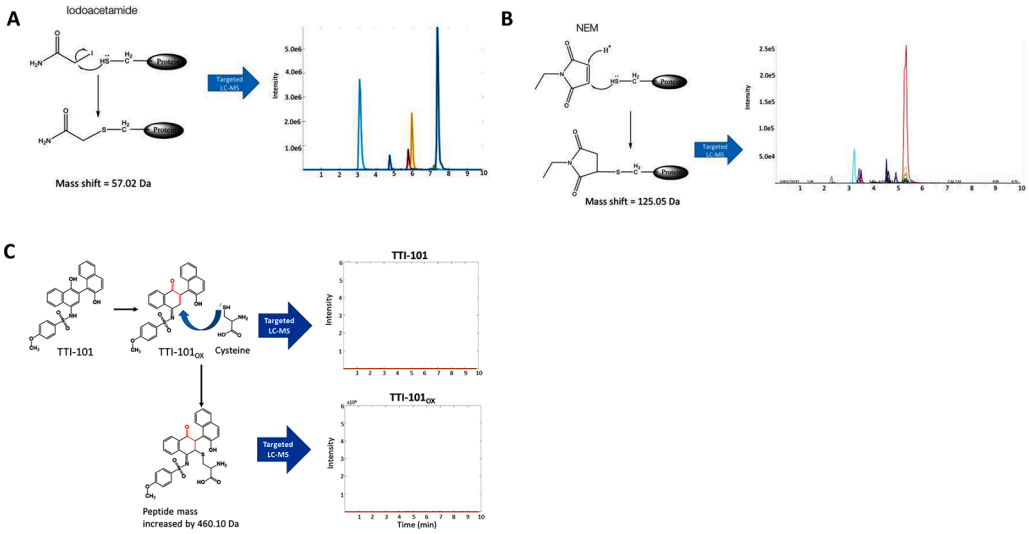

Fig. 4. Results of alkylation studies of STAT3 by iodoacetamide, NEM and TTI-101. Schematic depicting chemistry of possible alkylation of STAT3 by iodoacetamide the results of LC-MS chromatograms of STAT3 peptides demonstrating alkylated peptides, as predicted from the chemistry. Schematic depicting chemistry of possible alkylation of STAT3 by NEM the results of LC-MS chromatograms of STAT3 peptides demonstrating alkylated peptides, as predicted from the chemistry. Schematic depicting the chemistry of possible alkylation of STAT3 by TTI-101. The LC-MS chromatograms of STAT3 peptides, that, shows no MRM signal for predicted peptide adducts, indicating that no peptides were alkylated.

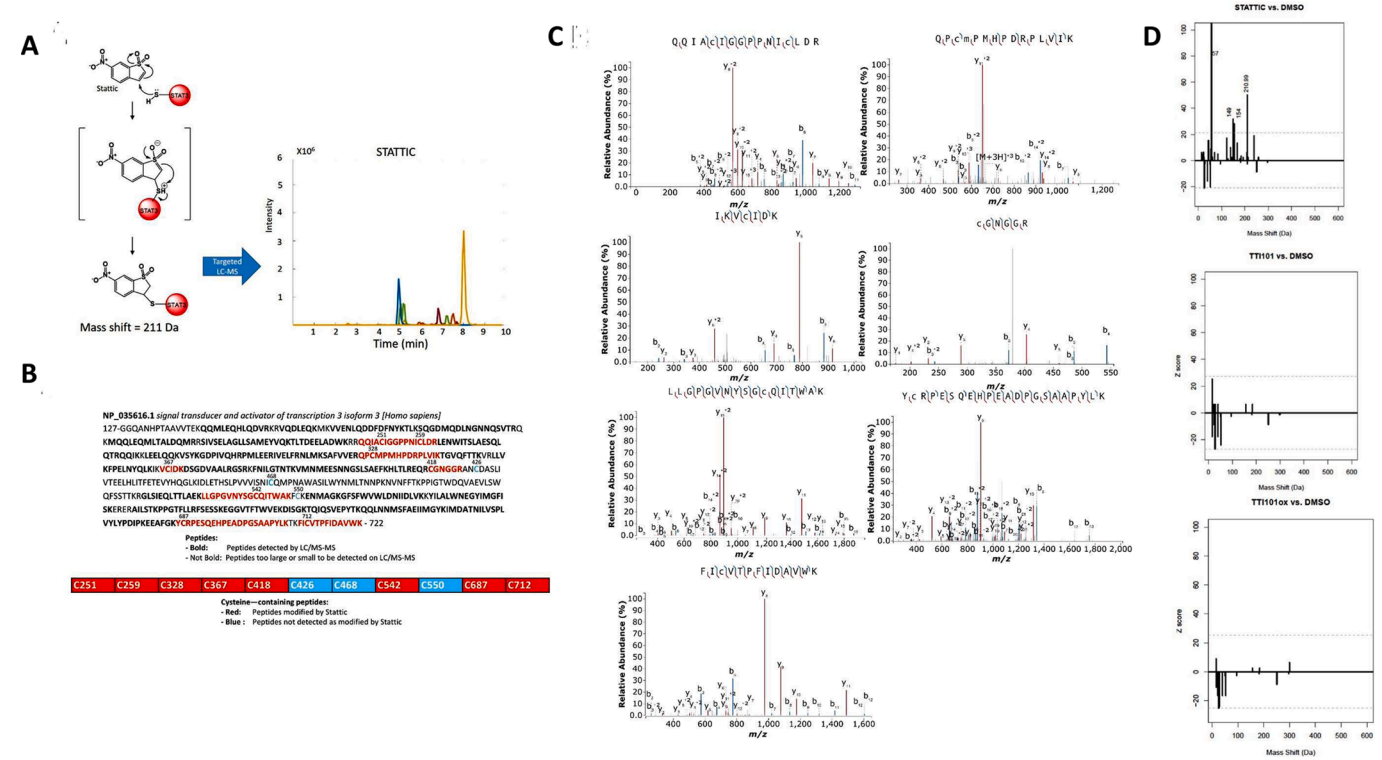

Fig. 5. Alkylation of STAT3 by Stattic. Schematic depicting chemistry of possible alkylation of STAT3 by Stattic and results of LC-MS chromatograms of STAT3 peptides of alkylated peptides, as predicted from reaction chemistry. Results of LC-MS/MS demonstrating covalent modification of STAT3 by Stattic. Chromatograms show fragment ion analysis revealing alkylation of each cysteine-containing peptide, as indicated. Mass Spectra were annotated using IPSA [47]. Representative data of four independent experiments. Amino acid sequence of STAT3βtr indicating cysteine residues modified. Red residues indicates cysteine-containing tryptic fragments identified by LC-MS/MS, with some peptides containing more than one modified cysteine. Bolded residues are within tryptic fragments that can be identified by LC-MS/MS. Residues that are not bolded are within tryptic fragments that are either too large or too small to be detected. Z-score histograms comparing mass shifts of STAT3 peptides incubated with Stattic, TTI-101, or TTI-101ox vs. STAT3 incubated with DMSO. The dotted line indicates the cutoff for a significant Z-score. The peptide mass peak shifted by 211 Da represents the predicted addition of Stattic as a chemical adduct; no significant mass shifts were observed with TTI-101 or with TTI-101ox indicating that neither forms chemical adducts with STAT3.

molecule STAT3 inhibitors in clinical-stage development [4–6]. To assess whether TTI-101 causes peripheral neuropathy, male C57BL/6 mice were treated with 7 doses of TTI-101 (50 mg/kg i.p. every other day) and sensitivity to mechanical stimulation was followed over time using von Frey hairs. Administration of TTI-101 alone had no effect on mechanical sensitivity (Fig. 6**A**). To investigate whether TTI-101 aggravates existing neuropathic pain, we used the cisplatin model of chemotherapy-induced peripheral neuropathy (CIPN). This model was selected because we showed previously that it is mediated by mitochondrial damage in the peripheral nervous system [17,29]. Mice were treated with two cycles of cisplatin (5 daily doses of 2.3 mg/kg followed by 5 days rest), which induces mechanical allodynia (Fig. 6**B**) that lasts

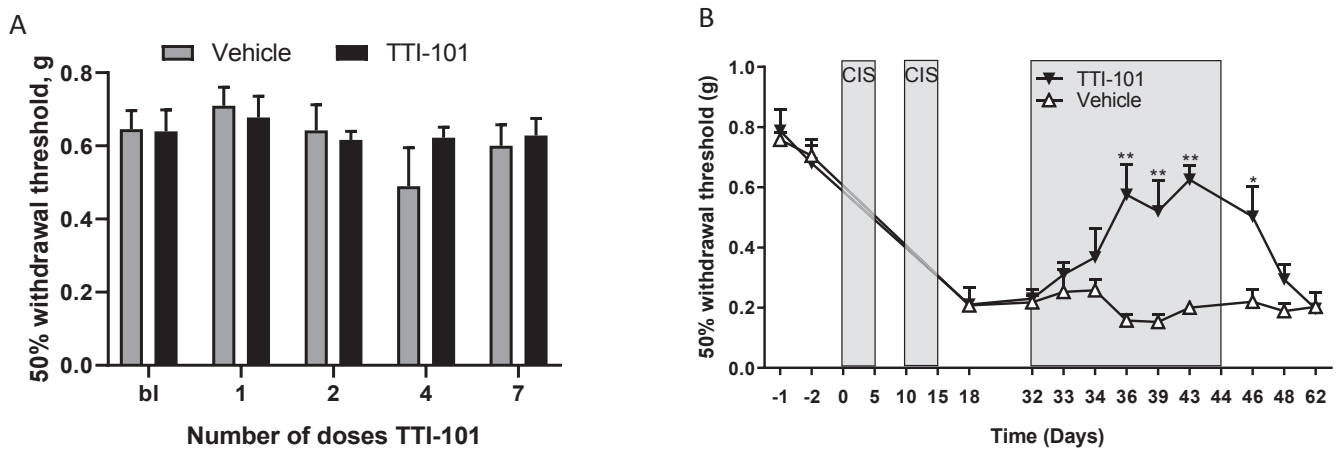

Fig. 6. TTI-101 does not cause mechanical allodynia; rather, it reverses mechanical allodynia caused by cisplatin. A. Male C57/Bl6 mice (n = 8 per group) received TTI-101 (50 mg/kg i.p. every other day) and mechanical allodynia was assessed using von Frey hairs and the up-and-down method. B. Male C57/Bl6 mice (n = 4 per group) were treated with cisplatin (two rounds of 5 daily doses of 2.3 mg/kg i.p. followed by 5 days of rest). Dosing with TTI-101 (50 mg/kg i.p. every other day) started 17 days after the last dose of cisplatin. Data were analyzed by two-way ANOVA repeated measures. Time: $P < 0.001$; Group: $P < 0.001$; Interaction $P < 0.001$. **$P < 0.01$ Tukey multiple comparison test.

for at least 75 days [17]. TTI-101 administration (50 mg/kg i.p. every other day for a total of 7 doses) was started 17 days after the last dose of cisplatin, when mechanical allodynia had developed fully. TTI-101 administration markedly reduced cisplatin-induced mechanical allodynia (Fig. 6**B**). The beneficial effect of TTI-101 developed slowly over time—maximal inhibition was obtained after the 4th dose of TTI-101 and was maintained while dosing continued. Mechanical allodynia returned to levels similar to those in mice treated with cisplatin alone 4 days after the last dose of TTI-101.

3.5. TTI-101 suppresses SNI- induced mechanical allodynia

To determine whether the beneficial effect of TTI-101 is limited to CIPN or is more broadly applicable to other causes of neuropathic pain, we examined its effect on mechanical allodynia induced by SNI. SNI induces profound mechanical allodynia in male and female mice. Administration of TTI-101 in the SNI model reduced mechanical allodynia within 6 h of the first dose (Fig. 7**A**) and repeated dosing of TTI-101 over 14 days led to complete reversal of SNI-induced mechanical allodynia in male and female mice (Fig. 7**B**) that was sustained through day 52 of the experiment or 40 days after the last dose of TTI-101.

3.6. RNA-seq analysis of effect of TTI-101 on the DRG transcriptome in cisplatin-treated mice

To determine whether the beneficial effect of TTI-101 on CIPN is associated with changes in the transcriptome and, in particular, in expression of STAT3 target genes, we performed RNA-seq analysis on dorsal root ganglia (DRG). Mice were treated with cisplatin followed by TTI-101 as in Fig. 6 and lumbar DRG were collected at 4 Hrs after the fourth dose of TTI-101 or vehicle. Comparison of the transcriptome in DRG from mice treated with cisplatin vs. PBS showed that cisplatin changed the expression of 1,973 genes (675 down, 1,298 up; Fig. 8**A**). TTI-101 administration to cisplatin-treated mice changed expression of 1,713 genes (1,416 down, 297 up) vs. mice treated with cisplatin alone. Notably, the 443 genes that were altered in both groups (PBS vs. Cis and Cis vs. Cis + TTI-101) showed an overall opposite expression pattern between groups, indicating that TTI-101 administration normalized the

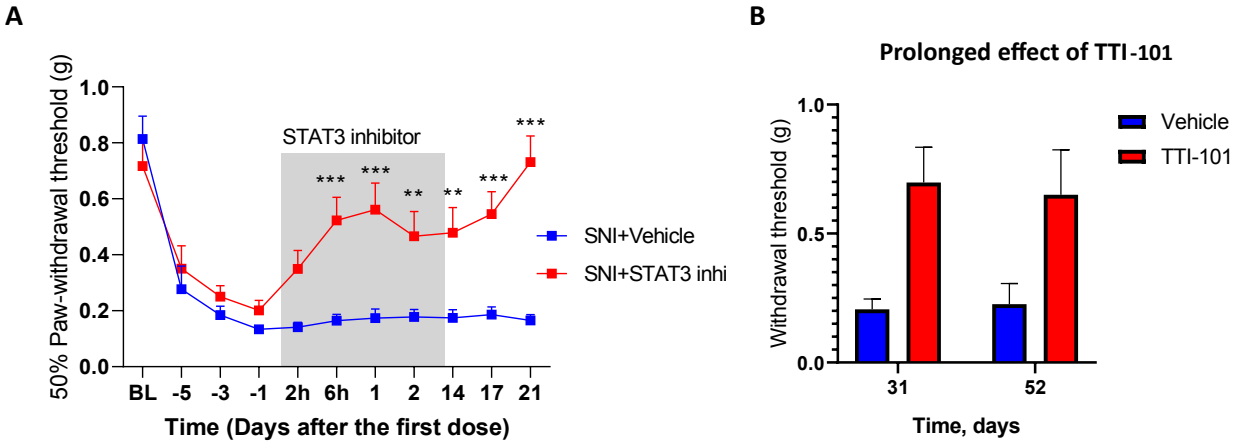

Fig. 7. STAT3 inhibitor reverses SNI-induced allodynia. Male and female mice underwent SNI surgery and were treated with TTI-101 (Males: n = 5; females: n = 6) or vehicle (Males: n = 4; Females: n = 6) by oral gavage for 6 doses every other day from day 10 after SNI. Mechanical allodynia in male and female mice. Data are shown as mean ± SEM and were analyzed using two-way ANOVA followed by Sidak's post-hoc test. * $P < 0.05$. No signs of mechanical allodynia at 31 and 52 days after start of TTI-101 treatment (19 and 40 days after the last dose). Data are from 4 vehicle-treated and 5 TTI-101-treated male mice per group). Two-way ANOVA followed by Sidak's post-hoc test: $P < 0.05$.

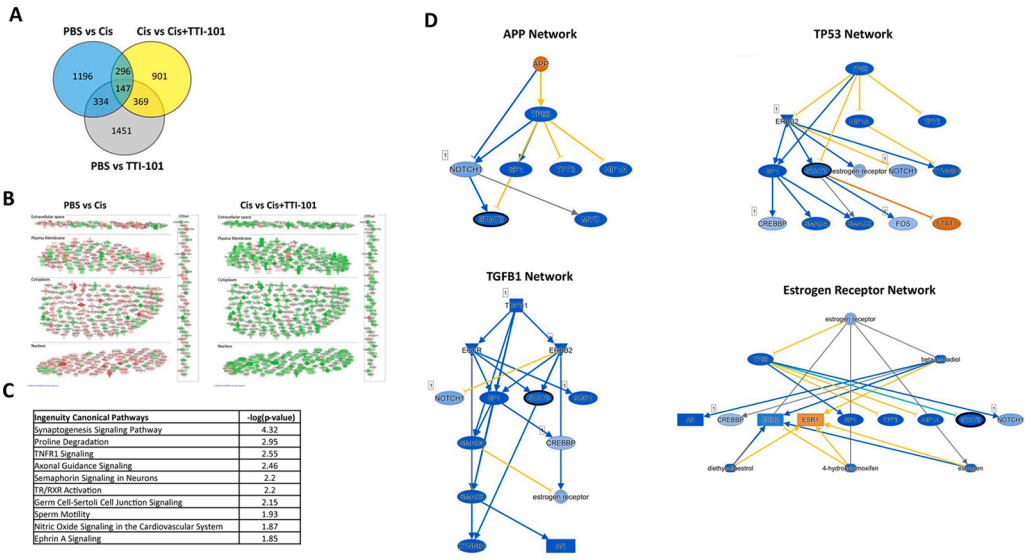

Ingenuity Canonical Pathways	-log(p-value)
Synaptogenesis Signaling Pathway	4.32
Proline Degradation	2.95
TNFR1 Signaling	2.55
Axonal Guidance Signaling	2.46
Semaphorin Signaling in Neurons	2.2
TR/RXR Activation	2.2
Germ Cell-Sertoli Cell Junction Signaling	2.15
Sperm Motility	1.93
Nitric Oxide Signaling in the Cardiovascular System	1.87
Ephrin A Signaling	1.85

Fig. 8. Effect of TTI-101 on the DRG transcriptome of cisplatin-treated mice. Genes differentially expressed among groups is shown in a Venn diagram. Expression of 1,973 genes was changed in response to cisplatin when compared to the PBS mice (PBS vs. Cis; n = 3 male mice per group). Expression of 1,713 genes was changed in response to TTI-101 administration vs. mice treated with cisplatin alone (Cis vs. Cis + TTI-101). A cutoff of (−0.2 < log2 Fold Change < 0.2) and p = 0.1 was used for the analysis. Expression of 2,154 genes was changes in response to TTI-101 administration compared to PBS mice (PBS vs TTI-101). Subcellular clustering of 443 overlapping genes showing directionality of expression. Up-regulated and down-regulated genes are highlighted in red and green, respectively. Gray indicates effect cannot be predicted. Top IPA canonical pathways along with –log (p-value) assigned to 443 common genes between PBS vs. Cis and Cis vs. Cis + TTI-101 mice. Mechanistic networks of four upstream regulators involving STAT3 as an intermediate regulator. Note that STAT3 (black outline) is an intermediate regulator in all networks and it is predicted to be inhibited. Color orange and blue indicate activation or inhibition respectively. Yellow arrow represents inconsistent relationship when the expected direction is different from direction observed.

expression of genes whose expression was altered in cisplatin-treated mice (Fig. 8**B** and Table 1).

Ingenuity pathway analysis (IPA) focused on canonical pathways (Fig. 8**C**) and showed that the 443 genes were mainly associated with neuronal health and survival pathways (namely synaptogenesis signaling pathways, TNFR signaling, axonal guidance signaling, Semaphorin Signaling in Neurons, Ephrin signaling). Upstream regulator analysis of the 1,713 differentially expressed genes (DEG) that changed with TTI-101 administration revealed huntingtin (HTT), amyloid beta precursor protein (APP), TP53, TGFβ1, and estrogen receptor as the top five upstream regulators driving downstream changes (**Table 2**). The mechanistic network of four regulators identified STAT3 as an intermediate regulator. Consistent with the activity of TTI-101 as a STAT3 inhibitor, STAT3 activity was reduced in all networks (Fig. 8**D**). For example, for the TP53 network, 14 regulators were part of the mechanistic network which together influence expression of 481 genes and out of these 481 genes, 64 target genes are regulated by STAT3.

To gain further insight into potential mechanisms underlying TTI-101′s reversal of CIPN, we used IPA to perform a comparison analysis (Fig. 9**A**). IPA identified VEGF as the top upstream regulator different between the groups—PBS vs. Cis and Cis vs. Cis + TTI-101. Specifically, IPA predicted activation of VEGF signaling in mice treated with cisplatin as compared to PBS. This pathway was inhibited when cisplatin-treated mice received TTI-101. The heat map in Fig. 9**B** shows the effect of TTI-101 administration on the target genes in VEGF signaling network.

4. Discussion

Small-molecule inhibitors that target the SH2 domain of STAT3 have been proposed recently as an example of synthetic lethality; upon STAT3 binding, they induce formation of proteotoxic aggregates that inhibit mitochondrial function leading to cell death, especially in cancer cells experiencing metabolic stress [6]. Perhaps, not surprisingly, cancer patients enrolled in Phase I/II clinical studies of some drugs within this class have experienced SAE, such as lactic acidosis and peripheral neuropathy, which are clinical manifestations of mitochondrial toxicity; these SAE have halted further patient enrollment. Our group developed TTI-101, a competitive inhibitor of STAT3 designed to target the pY-peptide binding site within STAT3′s SH2 domain and to directly block two key steps in its activation—recruitment to activated cytokine receptor complexes and homodimerization. The studies reported here were undertaken to determine if TTI-101 targets STAT3′s mitochondrial function, causes STAT3 aggregation, or induces peripheral neuropathy. We report that TTI-101 does not affect mitochondrial function, does not cause STAT3 aggregation through chemical modification or other means, and does not induce pain measured as mechanical allodynia. In fact, TTI-101 administration unexpectedly suppressed mechanical allodynia induced by the chemotherapeutic agent cisplatin, indicating it may be of special benefit when administered to cancer patients at risk of developing chemotherapy-induced peripheral neuropathy (CIPN).

While the Otsuka compounds were unavailable to us for study, we examined two compounds (WP1066 and cryptotanshinone) previously demonstrated to markedly affect mitochondrial function for evidence of covalent modification of STAT3, in particular, alkylation. LC-MS/MS of STAT3 protein incubated with WP1066 and cryptotanshinone revealed no alkylation at cysteine sites. In contrast, Stattic, which did not affect mitochondrial function, alkylated STAT3 at all detectable cysteines. STA21, which emerged from a virtual ligand screen for compounds that bind the STAT3 SH2 domain [30], behaved in manner identical to TTI-101; it neither alkylated STAT3 nor induced mitochondrial toxicity. Thus, the ability of STAT3 inhibitors to cause STAT3 aggregation and mitochondrial toxicity is not related to their ability to covalently modify STAT3 and their precise mechanism for inducing STAT3 aggregation remains uncertain.

We previously demonstrated that administration of TTI-101 to rats for 28 days (up to a dose of 200 mg/kg/day) and to dogs (up to a dose of 100 mg/kg/day) did not cause any metabolic abnormalities including lactic acidosis. Increasing evidence indicates that, in addition to lactic acidosis, mitochondrial dysfunction plays a key role in the development of chemotherapy-induced neuropathic pain [31–33]. Peripheral neuropathy is one of the SAE that have been observed with some small-molecule STAT3 inhibitors in clinical-stage development [5]. Our current findings show that treatment of naïve mice with TTI-101 does not induce neuropathic pain in the von Frey test of mechanical allodynia (Fig. 6**A**), which is commonly used to assess for peripheral neuropathic pain in rodent models.

Table 1
Details on the overlapping genes that were altered in both groups, PBS vs Cis, and Cis vs Cis + TTI-101.

	Symbol	Entrez Gene Name	Location	PBS vs Cis		Cis vs Cis + TTI-101	
				log_2 Fold Change	Expr p-value	log_2 Fold Change	Expr p-value
1	6530402F18Rik	RIKEN cDNA 6530402F18 gene	Other	−0.27	0.07	−0.44	0.02
2	ABCA2	ATP binding cassette subfamily A member 2	Plasma Membrane	0.23	0.01	−0.42	0.04
3	ABCA3	ATP binding cassette subfamily A member 3	Plasma Membrane	0.28	0.00	−0.32	0.06
4	ABCA7	ATP binding cassette subfamily A member 7	Plasma Membrane	0.24	0.01	−0.36	0.03
5	ABCG4	ATP binding cassette subfamily G member 4	Plasma Membrane	0.24	0.00	−0.32	0.04
6	ABHD17A	abhydrolase domain containing 17A	Plasma Membrane	−0.23	0.00	−0.35	0.00
7	ABHD8	abhydrolase domain containing 8	Cytoplasm	−0.27	0.00	−0.21	0.06
8	ACACB	acetyl-CoA carboxylase beta	Cytoplasm	0.30	0.02	−0.30	0.04
9	ADAMTSL2	ADAMTS like 2	Extracellular Space	0.37	0.02	−0.31	0.08
10	ADAP1	ArfGAP with dual PH domains 1	Nucleus	−0.22	0.00	−0.23	0.05
11	ADCK2	aarF domain containing kinase 2	Cytoplasm	0.20	0.05	−0.30	0.02
12	AEBP1	AE binding protein 1	Nucleus	0.60	0.00	−0.23	0.08
13	AKNA	AT-hook transcription factor	Nucleus	0.54	0.00	−0.41	0.03
14	ALAD	aminolevulinate dehydratase	Cytoplasm	0.30	0.01	−0.43	0.01
15	ALDH2	aldehyde dehydrogenase 2 family member	Cytoplasm	0.23	0.00	−0.34	0.02
16	ALDH4A1	aldehyde dehydrogenase 4 family member A1	Cytoplasm	0.35	0.00	−0.29	0.05
17	ALOX5	arachidonate 5-lipoxygenase	Cytoplasm	0.76	0.00	−0.38	0.07
18	AMBRA1	autophagy and beclin 1 regulator 1	Cytoplasm	0.22	0.01	−0.32	0.02
19	AMOTL2	angiomotin like 2	Plasma Membrane	0.24	0.00	−0.31	0.01
20	AMPD2	adenosine monophosphate deaminase 2	Cytoplasm	0.24	0.00	−0.25	0.07
21	AMPD3	adenosine monophosphate deaminase 3	Cytoplasm	0.26	0.00	−0.21	0.08
22	ANKRD13B	ankyrin repeat domain 13B	Plasma Membrane	−0.26	0.01	−0.28	0.05
23	ANO1	anoctamin 1	Plasma Membrane	0.36	0.01	−0.33	0.04
24	AP5Z1	adaptor related protein complex 5 subunit zeta 1	Nucleus	0.24	0.01	−0.27	0.04
25	ARAP3	ArfGAP with RhoGAP domain, ankyrin repeat and PH domain 3	Cytoplasm	0.36	0.00	−0.24	0.07
26	ARHGEF10L	Rho guanine nucleotide exchange factor 10 like	Cytoplasm	−0.34	0.00	−0.28	0.05
27	ARHGEF2	Rho/Rac guanine nucleotide exchange factor 2	Cytoplasm	0.28	0.00	−0.22	0.05
28	ARID3A	AT-rich interaction domain 3A	Nucleus	0.29	0.05	−0.29	0.05
29	ARMC7	armadillo repeat containing 7	Cytoplasm	0.22	0.07	−0.35	0.02
30	ARMH3	armadillo like helical domain containing 3	Other	0.25	0.00	−0.28	0.09
31	ARRDC1	arrestin domain containing 1	Cytoplasm	0.22	0.01	−0.20	0.08
32	ATP1B2	ATPase Na+/K + transporting subunit beta 2	Plasma Membrane	0.25	0.00	−0.42	0.01
33	ATP2A3	ATPase sarcoplasmic/endoplasmic reticulum Ca2 + transporting 3	Cytoplasm	0.53	0.00	−0.49	0.00
34	ATP2B2	ATPase plasma membrane Ca2 + transporting 2	Plasma Membrane	0.39	0.00	−0.45	0.02
35	ATP6V1G2	ATPase H + transporting V1 subunit G2	Cytoplasm	0.23	0.00	−0.31	0.01
36	B230206H07Rik	RIKEN cDNA B230206H07 gene	Other	0.59	0.00	−0.38	0.07
37	BAG3	BCL2 associated athanogene 3	Cytoplasm	−0.27	0.00	−0.38	0.01
38	BCAR1	BCAR1 scaffold protein, Cas family member	Plasma Membrane	−0.23	0.03	−0.31	0.05
39	BCOR	BCL6 corepressor	Nucleus	0.28	0.00	−0.21	0.07
40	BRD3	bromodomain containing 3	Nucleus	0.34	0.00	−0.26	0.06
41	BRPF3	bromodomain and PHD finger containing 3	Cytoplasm	0.26	0.00	−0.22	0.05
42	C11orf24	chromosome 11 open reading frame 24	Extracellular Space	0.32	0.00	−0.31	0.08
43	C11orf98	chromosome 11 open reading frame 98	Other	−0.24	0.03	0.25	0.04
44	C15orf39	chromosome 15 open reading frame 39	Cytoplasm	0.37	0.05	−0.50	0.03
45	C1QC	complement C1q C chain	Extracellular Space	−0.38	0.01	0.52	0.01
46	C3AR1	complement C3a receptor 1	Plasma Membrane	−0.44	0.06	0.63	0.02
47	CACHD1	cache domain containing 1	Other	0.22	0.02	−0.29	0.08
48	CACNG5	calcium voltage-gated channel auxiliary subunit gamma 5	Plasma Membrane	0.41	0.00	−0.47	0.02
49	CAD	carbamoyl-phosphate synthetase 2, aspartate transcarbamylase, and dihydroorotase	Cytoplasm	0.22	0.03	−0.49	0.01
50	CAMK2B	calcium/calmodulin dependent protein kinase II beta	Cytoplasm	0.23	0.00	−0.28	0.03
51	CARMIL2	capping protein regulator and myosin 1 linker 2	Plasma Membrane	−0.29	0.00	−0.32	0.02
52	CASP1	caspase 1	Cytoplasm	−0.36	0.06	0.33	0.06

(*continued on next page*)

Table 1 (*continued*)

	Symbol	Entrez Gene Name	Location	PBS vs Cis		Cis vs Cis + TTI-101	
				log_2 Fold Change	Expr p-value	log_2 Fold Change	Expr p-value
53	CASR	calcium sensing receptor	Plasma Membrane	−0.36	0.09	0.33	0.07
54	CBLL1	Cbl proto-oncogene like 1	Nucleus	0.24	0.02	−0.30	0.07
55	CCDC88B	coiled-coil domain containing 88B	Nucleus	0.40	0.09	−0.44	0.08
56	CCDC88C	coiled-coil domain containing 88C	Cytoplasm	0.88	0.00	−0.44	0.04
57	CCDC92B	coiled-coil domain containing 92B	Other	−0.28	0.00	−0.31	0.03
58	CCN2	cellular communication network factor 2	Extracellular Space	0.36	0.03	−0.34	0.08
59	CDC42EP3	CDC42 effector protein 3	Cytoplasm	0.25	0.04	−0.30	0.02
60	CEP250	centrosomal protein 250	Nucleus	0.22	0.00	−0.21	0.07
61	CHD4	chromodomain helicase DNA binding protein 4	Nucleus	0.23	0.00	−0.24	0.08
62	CHD5	chromodomain helicase DNA binding protein 5	Nucleus	0.21	0.00	−0.35	0.01
63	CHERP	calcium homeostasis endoplasmic reticulum protein	Cytoplasm	0.24	0.01	−0.43	0.00
64	CHIC2	cysteine rich hydrophobic domain 2	Plasma Membrane	−0.21	0.07	0.23	0.08
65	CHPF	chondroitin polymerizing factor	Cytoplasm	−0.28	0.00	−0.24	0.05
66	CHST2	carbohydrate sulfotransferase 2	Cytoplasm	−0.25	0.00	−0.31	0.01
67	CIART	circadian associated repressor of transcription	Nucleus	0.53	0.02	0.37	0.04
68	CISD3	CDGSH iron sulfur domain 3	Cytoplasm	−0.23	0.00	0.21	0.04
69	CITED2	Cbp/p300 interacting transactivator with Glu/Asp rich carboxy-terminal domain 2	Nucleus	0.24	0.03	−0.27	0.05
70	CLIP2	CAP-Gly domain containing linker protein 2	Cytoplasm	−0.21	0.01	−0.33	0.03
71	CLSTN2	calsyntenin 2	Plasma Membrane	0.21	0.00	−0.26	0.08
72	CLSTN3	calsyntenin 3	Plasma Membrane	0.22	0.01	−0.29	0.07
73	CLUH	clustered mitochondria homolog	Cytoplasm	0.40	0.00	−0.41	0.03
74	CNTN2	contactin 2	Plasma Membrane	0.24	0.00	−0.41	0.02
75	CNTROB	centrobin, centriole duplication and spindle assembly protein	Cytoplasm	0.28	0.01	−0.27	0.05
76	COBLL1	cordon-bleu WH2 repeat protein like 1	Extracellular Space	0.25	0.03	−0.27	0.02
77	COL6A3	collagen type VI alpha 3 chain	Extracellular Space	0.43	0.00	−0.25	0.08
78	COMP	cartilage oligomeric matrix protein	Extracellular Space	0.39	0.00	−0.31	0.06
79	CORO6	coronin 6	Extracellular Space	0.25	0.02	−0.24	0.07
80	CORO7/CORO7-PAM16	coronin 7	Cytoplasm	0.32	0.00	−0.29	0.07
81	CPB1	carboxypeptidase B1	Extracellular Space	−0.26	0.04	0.26	0.06
82	CPSF1	cleavage and polyadenylation specific factor 1	Nucleus	0.54	0.00	−0.30	0.07
83	CRIP1	cysteine rich protein 1	Cytoplasm	−0.29	0.00	0.29	0.04
84	CRMP1	collapsin response mediator protein 1	Cytoplasm	0.27	0.00	−0.27	0.07
85	CRTC2	CREB regulated transcription coactivator 2	Nucleus	0.21	0.00	−0.27	0.01
86	CSDC2	cold shock domain containing C2	Cytoplasm	0.20	0.03	−0.46	0.01
87	CSF3R	colony stimulating factor 3 receptor	Plasma Membrane	0.63	0.00	−0.46	0.07
88	CSMD2	CUB and Sushi multiple domains 2	Other	0.25	0.03	−0.33	0.01
89	CSNK1G2	casein kinase 1 gamma 2	Cytoplasm	−0.23	0.00	−0.24	0.04
90	CSRNP1	cysteine and serine rich nuclear protein 1	Nucleus	0.32	0.07	−0.44	0.02
91	CTSE	cathepsin E	Cytoplasm	1.04	0.02	−0.65	0.00
92	Cux1	cut-like homeobox 1	Nucleus	0.24	0.00	−0.28	0.03
93	CX3CL1	C-X3-C motif chemokine ligand 1	Extracellular Space	0.33	0.01	−0.33	0.06
94	DAG1	dystroglycan 1	Plasma Membrane	0.21	0.00	−0.48	0.01
95	DAP	death associated protein	Cytoplasm	0.21	0.02	−0.23	0.03
96	DDX19A	DEAD-box helicase 19A	Nucleus	0.23	0.02	−0.24	0.06
97	DGCR2	DiGeorge syndrome critical region gene 2	Plasma Membrane	0.20	0.00	−0.27	0.08
98	DGKD	diacylglycerol kinase delta	Cytoplasm	0.23	0.01	−0.21	0.07
99	DHX34	DExH-box helicase 34	Other	0.24	0.02	−0.33	0.06
100	DIO2	iodothyronine deiodinase 2	Cytoplasm	−0.47	0.04	−0.59	0.01
101	DISP1	dispatched RND transporter family member 1	Plasma Membrane	0.28	0.00	−0.22	0.06
102	DLC1	DLC1 Rho GTPase activating protein	Cytoplasm	0.24	0.00	−0.30	0.07
103	DLGAP3	DLG associated protein 3	Cytoplasm	−0.28	0.01	−0.36	0.05
104	DNAJC15	DnaJ heat shock protein family (Hsp40) member C15	Cytoplasm	−0.22	0.02	0.21	0.09
105	DNM1	dynamin 1	Cytoplasm	−0.22	0.03	−0.27	0.09
106	DNMT1	DNA methyltransferase 1	Nucleus	0.38	0.00	−0.24	0.05
107	DOCK1	dedicator of cytokinesis 1	Cytoplasm	0.29	0.00	−0.36	0.02

(*continued on next page*)

Table 1 (*continued*)

	Symbol	Entrez Gene Name	Location	PBS vs Cis		Cis vs Cis + TTI-101	
				log_2 Fold Change	Expr p-value	log_2 Fold Change	Expr p-value
108	DOCK6	dedicator of cytokinesis 6	Cytoplasm	0.41	0.00	−0.22	0.10
109	DOCK8	dedicator of cytokinesis 8	Cytoplasm	0.45	0.00	−0.30	0.01
110	DOK3	docking protein 3	Cytoplasm	0.48	0.02	−0.43	0.07
111	DOP1B	DOP1 leucine zipper like protein B	Cytoplasm	0.28	0.01	−0.41	0.03
112	DPYSL4	dihydropyrimidinase like 4	Cytoplasm	0.34	0.00	−0.25	0.02
113	DUS3L	dihydrouridine synthase 3 like	Other	0.23	0.00	−0.20	0.05
114	DUSP15	dual specificity phosphatase 15	Cytoplasm	0.28	0.01	−0.31	0.05
115	E2F2	E2F transcription factor 2	Nucleus	0.52	0.00	−0.33	0.09
116	EDC4	enhancer of mRNA decapping 4	Cytoplasm	0.43	0.00	−0.25	0.08
117	EFHC1	EF-hand domain containing 1	Cytoplasm	−0.29	0.04	0.34	0.03
118	EGR2	early growth response 2	Nucleus	0.28	0.04	−0.52	0.02
119	ELANE	elastase, neutrophil expressed	Extracellular Space	0.86	0.00	−0.72	0.03
120	ELMO1	engulfment and cell motility 1	Cytoplasm	0.26	0.00	−0.22	0.08
121	EMC1	ER membrane protein complex subunit 1	Plasma Membrane	0.27	0.00	−0.22	0.10
122	EMCN	endomucin	Extracellular Space	−0.22	0.02	0.29	0.03
123	EPHA2	EPH receptor A2	Plasma Membrane	0.30	0.09	−0.43	0.03
124	ERBB2	erb-b2 receptor tyrosine kinase 2	Plasma Membrane	0.26	0.01	−0.35	0.01
125	ERBB3	erb-b2 receptor tyrosine kinase 3	Plasma Membrane	0.26	0.00	−0.27	0.01
126	ERMAP	erythroblast membrane associated protein (Scianna blood group)	Cytoplasm	1.31	0.00	−0.54	0.06
127	ESS2	ess-2 splicing factor homolog	Nucleus	0.28	0.00	−0.22	0.09
128	EXOSC9	exosome component 9	Nucleus	−0.20	0.03	0.20	0.09
129	F2RL2	coagulation factor II thrombin receptor like 2	Plasma Membrane	−0.23	0.00	0.22	0.04
130	F5	coagulation factor V	Extracellular Space	0.76	0.00	−0.45	0.04
131	F630028O10Rik	RIKEN cDNA F630028O10 gene	Other	0.82	0.00	−0.47	0.07
132	FABP7	fatty acid binding protein 7	Cytoplasm	−0.55	0.00	−0.28	0.03
133	FAM20A	FAM20A golgi associated secretory pathway pseudokinase	Extracellular Space	0.35	0.00	−0.31	0.04
134	FAM222B	family with sequence similarity 222 member B	Nucleus	0.41	0.00	−0.36	0.05
135	FAM234A	family with sequence similarity 234 member A	Plasma Membrane	0.37	0.00	−0.31	0.02
136	FAM43B	family with sequence similarity 43 member B	Other	−0.25	0.02	−0.35	0.05
137	FARSB	phenylalanyl-tRNA synthetase subunit beta	Cytoplasm	−0.23	0.00	0.22	0.07
138	FAT1	FAT atypical cadherin 1	Plasma Membrane	0.45	0.00	−0.40	0.04
139	FBLN1	fibulin 1	Extracellular Space	0.40	0.00	−0.34	0.02
140	FBLN7	fibulin 7	Extracellular Space	0.35	0.01	−0.31	0.08
141	FBXO42	F-box protein 42	Other	0.21	0.00	−0.28	0.07
142	FERMT3	fermitin family member 3	Cytoplasm	0.67	0.00	−0.48	0.06
143	FGGY	FGGY carbohydrate kinase domain containing	Other	−0.22	0.04	0.24	0.07
144	FICD	FIC domain containing	Nucleus	0.24	0.00	−0.39	0.02
145	FLOT1	flotillin 1	Plasma Membrane	0.25	0.00	−0.25	0.07
146	FLT1	fms related tyrosine kinase 1	Plasma Membrane	0.29	0.00	−0.50	0.00
147	FMN2	formin 2	Cytoplasm	−0.24	0.00	−0.26	0.04
148	FMNL3	formin like 3	Cytoplasm	0.26	0.05	−0.25	0.09
149	Folh1	folate hydrolase 1	Plasma Membrane	−0.28	0.00	0.28	0.01
150	FRMPD1	FERM and PDZ domain containing 1	Cytoplasm	0.27	0.00	−0.37	0.04
151	FRYL	FRY like transcription coactivator	Other	0.43	0.00	−0.24	0.09
152	FSCN1	fascin actin-bundling protein 1	Cytoplasm	−0.25	0.02	−0.41	0.00
153	GAA	glucosidase alpha, acid	Cytoplasm	0.35	0.00	−0.40	0.03
154	GAS2L1	growth arrest specific 2 like 1	Cytoplasm	−0.32	0.00	−0.27	0.06
155	GATB	glutamyl-tRNA amidotransferase subunit B	Cytoplasm	−0.22	0.02	0.22	0.09
156	GBF1	golgi brefeldin A resistant guanine nucleotide exchange factor 1	Cytoplasm	0.33	0.00	−0.31	0.10
157	GCN1	GCN1 activator of EIF2AK4	Cytoplasm	0.25	0.01	−0.34	0.06
158	GDF11	growth differentiation factor 11	Extracellular Space	−0.25	0.00	−0.21	0.05
159	GDPD5	glycerophosphodiester phosphodiesterase domain containing 5	Plasma Membrane	−0.25	0.00	−0.22	0.03
160	GLRX	glutaredoxin	Cytoplasm	−0.20	0.01	0.22	0.06

(*continued on next page*)

Table 1 (*continued*)

	Symbol	Entrez Gene Name	Location	PBS vs Cis		Cis vs Cis + TTI-101	
				log_2 Fold Change	Expr p-value	log_2 Fold Change	Expr p-value
161	Gm12696	predicted gene 12,696	Other	−0.39	0.00	0.27	0.08
162	Gm16907	predicted gene, 16,907	Other	0.59	0.01	0.45	0.02
163	GNG7	G protein subunit gamma 7	Plasma Membrane	0.23	0.01	−0.38	0.01
164	GPC1	glypican 1	Plasma Membrane	−0.20	0.00	−0.23	0.05
165	GPD1	glycerol-3-phosphate dehydrogenase 1	Cytoplasm	−0.20	0.03	−0.25	0.02
166	GPR153	G protein-coupled receptor 153	Plasma Membrane	−0.25	0.01	−0.26	0.06
167	GRINA	glutamate ionotropic receptor NMDA type subunit associated protein 1	Other	0.37	0.00	−0.30	0.07
168	GTF3A	general transcription factor IIIA	Nucleus	0.29	0.04	−0.29	0.07
169	GUCY1A1	guanylate cyclase 1 soluble subunit alpha 1	Cytoplasm	0.33	0.01	−0.27	0.05
170	GYPC	glycophorin C (Gerbich blood group)	Plasma Membrane	0.37	0.00	−0.39	0.01
171	HCFC1	host cell factor C1	Nucleus	0.32	0.00	−0.39	0.04
172	HCN2	hyperpolarization activated cyclic nucleotide gated potassium and sodium channel 2	Plasma Membrane	−0.35	0.06	−0.33	0.09
173	HCN4	hyperpolarization activated cyclic nucleotide gated potassium channel 4	Plasma Membrane	−0.20	0.06	−0.36	0.02
174	HDDC2	HD domain containing 2	Cytoplasm	−0.27	0.00	0.22	0.08
175	HELZ	helicase with zinc finger	Nucleus	0.24	0.01	−0.21	0.09
176	HEMGN	hemogen	Nucleus	1.31	0.00	−0.69	0.03
177	HGF	hepatocyte growth factor	Extracellular Space	−0.32	0.00	0.28	0.04
178	HHATL	hedgehog acyltransferase like	Cytoplasm	0.20	0.04	−0.24	0.09
179	HIVEP1	HIVEP zinc finger 1	Nucleus	0.21	0.01	−0.34	0.05
180	HOXA7	homeobox A7	Nucleus	0.25	0.01	−0.35	0.02
181	HOXC10	homeobox C10	Nucleus	0.29	0.01	−0.28	0.04
182	HPS4	HPS4 biogenesis of lysosomal organelles complex 3 subunit 2	Cytoplasm	0.30	0.00	−0.28	0.04
183	HSP90AA1	heat shock protein 90 alpha family class A member 1	Cytoplasm	−0.26	0.00	0.21	0.07
184	Ifi27	interferon, alpha-inducible protein 27	Cytoplasm	−0.23	0.00	0.22	0.03
185	Ifi27l2a/Ifi27l2b	interferon, alpha-inducible protein 27 like 2A	Cytoplasm	−0.38	0.02	0.70	0.09
186	IFRD2	interferon related developmental regulator 2	Nucleus	0.64	0.00	−0.53	0.01
187	IGLON5	IgLON family member 5	Other	−0.23	0.01	−0.32	0.02
188	INCENP	inner centromere protein	Nucleus	0.61	0.00	−0.38	0.03
189	INPP5E	inositol polyphosphate-5-phosphatase E	Cytoplasm	0.21	0.01	−0.20	0.08
190	INSRR	insulin receptor related receptor	Plasma Membrane	0.62	0.01	−0.43	0.04
191	INSYN1	inhibitory synaptic factor 1	Plasma Membrane	−0.32	0.00	−0.31	0.05
192	IPO4	importin 4	Nucleus	0.26	0.00	−0.26	0.09
193	IRF2BP1	interferon regulatory factor 2 binding protein 1	Nucleus	−0.26	0.01	−0.37	0.03
194	IRF2BPL	interferon regulatory factor 2 binding protein like	Nucleus	−0.25	0.01	−0.30	0.05
195	ITGA2B	integrin subunit alpha 2b	Plasma Membrane	0.47	0.01	−0.61	0.01
196	ITPR3	inositol 1,4,5-trisphosphate receptor type 3	Cytoplasm	0.33	0.00	−0.43	0.02
197	KCNA1	potassium voltage-gated channel subfamily A member 1	Plasma Membrane	0.22	0.01	−0.31	0.07
198	KIAA1522	KIAA1522	Other	−0.21	0.01	−0.30	0.06
199	KIAA1549L	KIAA1549 like	Cytoplasm	0.20	0.01	−0.53	0.00
200	KMT2D	lysine methyltransferase 2D	Nucleus	0.20	0.08	−0.24	0.06
201	KNDC1	kinase non-catalytic C-lobe domain containing 1	Plasma Membrane	0.26	0.01	−0.44	0.03
202	LAMA5	laminin subunit alpha 5	Extracellular Space	0.37	0.00	−0.32	0.04
203	LAMC3	laminin subunit gamma 3	Extracellular Space	0.49	0.00	−0.50	0.06
204	LDLR	low density lipoprotein receptor	Plasma Membrane	0.39	0.00	−0.33	0.08
205	LGALS1	galectin 1	Extracellular Space	−0.31	0.00	0.26	0.06
206	LIMK1	LIM domain kinase 1	Cytoplasm	−0.29	0.00	−0.28	0.03
207	LITAF	lipopolysaccharide induced TNF factor	Nucleus	0.24	0.00	−0.20	0.05
208	LOC	proline dehydrogenase 1	Cytoplasm	0.23	0.04	0.49	0.01
209	LRP1	LDL receptor related protein 1	Plasma Membrane	0.41	0.00	−0.36	0.01
210	LRRC32	leucine rich repeat containing 32	Plasma Membrane	0.42	0.01	−0.37	0.10
211	LRRK1	leucine rich repeat kinase 1	Cytoplasm	0.27	0.01	−0.22	0.05
212	LRRN3	leucine rich repeat neuronal 3	Extracellular Space	−0.22	0.02	0.21	0.07
213	LSM7		Nucleus	−0.25	0.02	0.25	0.07

(*continued on next page*)

Table 1 (*continued*)

	Symbol	Entrez Gene Name	Location	PBS vs Cis		Cis vs Cis + TTI-101	
				log_2 Fold Change	Expr p-value	log_2 Fold Change	Expr p-value
		LSM7 homolog, U6 small nuclear RNA and mRNA degradation associated					
214	MADD	MAP kinase activating death domain	Cytoplasm	0.20	0.01	−0.23	0.10
215	MAP3K14	mitogen-activated protein kinase kinase kinase 14	Cytoplasm	0.26	0.09	−0.25	0.09
216	MAP4K2	mitogen-activated protein kinase kinase kinase kinase 2	Cytoplasm	0.31	0.00	−0.27	0.01
217	MAP7D1	MAP7 domain containing 1	Cytoplasm	−0.22	0.01	−0.25	0.05
218	MAPK7	mitogen-activated protein kinase 7	Cytoplasm	0.23	0.01	−0.32	0.01
219	MARK4	microtubule affinity regulating kinase 4	Cytoplasm	−0.23	0.06	−0.33	0.08
220	MAST4	microtubule associated serine/threonine kinase family member 4	Other	0.31	0.01	−0.42	0.03
221	MCC	MCC regulator of WNT signaling pathway	Cytoplasm	0.29	0.00	−0.21	0.06
222	MDC1	mediator of DNA damage checkpoint 1	Nucleus	0.31	0.00	−0.30	0.04
223	MED15	mediator complex subunit 15	Nucleus	0.36	0.00	−0.37	0.05
224	MEX3D	mex-3 RNA binding family member D	Nucleus	−0.28	0.01	−0.29	0.07
225	MFSD2B	major facilitator superfamily domain containing 2B	Plasma Membrane	0.76	0.00	−0.32	0.08
226	MMP15	matrix metallopeptidase 15	Extracellular Space	−0.28	0.00	−0.44	0.01
227	MMP9	matrix metallopeptidase 9	Extracellular Space	0.86	0.00	−0.80	0.00
228	MPO	myeloperoxidase	Cytoplasm	1.26	0.00	−0.96	0.03
229	MRC2	mannose receptor C type 2	Plasma Membrane	0.23	0.00	−0.23	0.04
230	MRGPRX4	MAS related GPR family member X4	Plasma Membrane	−0.27	0.01	0.26	0.04
231	MRVI1	murine retrovirus integration site 1 homolog	Cytoplasm	0.36	0.00	−0.35	0.04
232	MTSS2	MTSS I-BAR domain containing 2	Plasma Membrane	−0.31	0.00	−0.38	0.01
233	MXD1	MAX dimerization protein 1	Nucleus	0.40	0.01	−0.35	0.07
234	MYO1D	myosin ID	Cytoplasm	0.33	0.00	−0.32	0.07
235	MYO1F	myosin IF	Cytoplasm	0.63	0.00	−0.39	0.06
236	MYO7A	myosin VIIA	Cytoplasm	0.29	0.00	−0.24	0.08
237	MYPOP	Myb related transcription factor, partner of profilin	Nucleus	−0.25	0.00	−0.29	0.02
238	NAA80	N(alpha)-acetyltransferase 80, NatH catalytic subunit	Cytoplasm	0.25	0.00	−0.38	0.01
239	Naip1 (includes others)	NLR family, apoptosis inhibitory protein 1	Cytoplasm	0.56	0.01	0.30	0.08
240	NAT8L	N-acetyltransferase 8 like	Cytoplasm	−0.23	0.00	−0.36	0.02
241	NCSTN	nicastrin	Plasma Membrane	0.30	0.00	−0.25	0.07
242	NDUFA3	NADH:ubiquinone oxidoreductase subunit A3	Cytoplasm	−0.21	0.00	0.22	0.06
243	NDUFAF4	NADH:ubiquinone oxidoreductase complex assembly factor 4	Cytoplasm	−0.21	0.01	0.20	0.04
244	NECTIN1	nectin cell adhesion molecule 1	Plasma Membrane	−0.42	0.00	−0.36	0.07
245	NFAM1	NFAT activating protein with ITAM motif 1	Plasma Membrane	0.81	0.00	−0.43	0.09
246	NFATC1	nuclear factor of activated T cells 1	Nucleus	0.32	0.01	−0.30	0.05
247	NFE2	nuclear factor, erythroid 2	Nucleus	1.09	0.00	−0.61	0.03
248	NLGN2	neuroligin 2	Plasma Membrane	−0.25	0.01	−0.32	0.03
249	NLGN3	neuroligin 3	Plasma Membrane	0.33	0.00	−0.34	0.00
250	NMD3	NMD3 ribosome export adaptor	Nucleus	−0.21	0.01	0.26	0.01
251	NOL6	nucleolar protein 6	Nucleus	0.25	0.00	−0.39	0.05
252	NOTCH2	notch receptor 2	Plasma Membrane	0.31	0.00	−0.27	0.01
253	Nppb	natriuretic peptide type B	Other	−0.40	0.02	0.34	0.05
254	NPTXR	neuronal pentraxin receptor	Plasma Membrane	−0.22	0.01	−0.29	0.08
255	NR1D1	nuclear receptor subfamily 1 group D member 1	Nucleus	0.36	0.01	−0.29	0.02
256	NR4A2	nuclear receptor subfamily 4 group A member 2	Nucleus	0.27	0.03	−0.29	0.09
257	NRSN2	neurensin 2	Plasma Membrane	0.58	0.00	−0.38	0.07
258	NRXN2	neurexin 2	Plasma Membrane	−0.26	0.01	−0.32	0.06
259	NUDCD1	NudC domain containing 1	Nucleus	−0.20	0.02	0.20	0.07
260	NUMA1	nuclear mitotic apparatus protein 1	Nucleus	0.34	0.00	−0.26	0.08
261	NUP188	nucleoporin 188	Nucleus	0.29	0.00	−0.21	0.08
262	OGDH	oxoglutarate dehydrogenase	Cytoplasm	0.36	0.00	−0.34	0.05
263	OGDHL	oxoglutarate dehydrogenase like	Other	0.25	0.01	−0.27	0.08
264	OLFM2	olfactomedin 2	Cytoplasm	0.31	0.00	−0.25	0.04
265	OPRM1	opioid receptor mu 1	Plasma Membrane	−0.28	0.00	0.23	0.01
266	OSBPL7	oxysterol binding protein like 7	Cytoplasm	0.27	0.00	−0.26	0.03
267	P2RY2	purinergic receptor P2Y2		0.31	0.00	−0.30	0.07

(*continued on next page*)

Table 1 (*continued*)

	Symbol	Entrez Gene Name	Location	PBS vs Cis		Cis vs Cis + TTI-101	
				log_2 Fold Change	Expr p-value	log_2 Fold Change	Expr p-value
			Plasma Membrane				
268	PALM	paralemmin	Plasma Membrane	−0.30	0.00	−0.27	0.05
269	PAPLN	papilin, proteoglycan like sulfated glycoprotein	Extracellular Space	0.20	0.09	−0.34	0.08
270	PC	pyruvate carboxylase	Cytoplasm	0.21	0.00	−0.30	0.04
271	PCIF1	PDX1 C-terminal inhibiting factor 1	Nucleus	0.25	0.01	−0.34	0.04
272	PCNX2	pecanex 2	Other	0.24	0.01	−0.37	0.04
273	PCSK1N	proprotein convertase subtilisin/kexin type 1 inhibitor	Extracellular Space	−0.32	0.10	−0.36	0.05
274	PDE4A	phosphodiesterase 4A	Cytoplasm	0.32	0.01	−0.39	0.02
275	PDGFRB	platelet derived growth factor receptor beta	Plasma Membrane	0.54	0.00	−0.27	0.09
276	PDK2	pyruvate dehydrogenase kinase 2	Cytoplasm	0.37	0.00	−0.31	0.10
277	Perm1	PPARGC1 and ESRR induced regulator, muscle 1	Other	0.52	0.01	−0.37	0.08
278	PGP	phosphoglycolate phosphatase	Cytoplasm	−0.35	0.00	−0.29	0.02
279	PHACTR4	phosphatase and actin regulator 4	Plasma Membrane	0.24	0.05	−0.26	0.07
280	PHLDA1	pleckstrin homology like domain family A member 1	Cytoplasm	−0.28	0.05	−0.32	0.05
281	PHRF1	PHD and ring finger domains 1	Nucleus	0.28	0.00	−0.32	0.06
282	PHYHIP	phytanoyl-CoA 2-hydroxylase interacting protein	Cytoplasm	0.34	0.03	−0.45	0.08
283	PIAS3	protein inhibitor of activated STAT 3	Nucleus	0.25	0.00	−0.20	0.04
284	PIK3CD	phosphatidylinositol-4,5-bisphosphate 3-kinase catalytic subunit delta	Cytoplasm	0.24	0.00	−0.41	0.01
285	PLA2R1	phospholipase A2 receptor 1	Plasma Membrane	−0.21	0.04	0.24	0.09
286	PLAGL2	PLAG1 like zinc finger 2	Nucleus	0.43	0.00	−0.31	0.06
287	PLEKHM1	pleckstrin homology and RUN domain containing M1	Cytoplasm	0.29	0.00	−0.26	0.06
288	PLPP3	phospholipid phosphatase 3	Plasma Membrane	0.26	0.00	−0.29	0.05
289	PLRG1	pleiotropic regulator 1	Nucleus	−0.21	0.01	0.21	0.07
290	PLTP	phospholipid transfer protein	Extracellular Space	0.49	0.00	−0.30	0.04
291	PLXNA2	plexin A2	Plasma Membrane	0.25	0.00	−0.28	0.08
292	PLXNB1	plexin B1	Plasma Membrane	0.28	0.02	−0.36	0.02
293	PLXNB3	plexin B3	Plasma Membrane	0.38	0.00	−0.30	0.05
294	PMEPA1	prostate transmembrane protein, androgen induced 1	Plasma Membrane	−0.27	0.00	−0.33	0.01
295	POLR2A	RNA polymerase II subunit A	Nucleus	0.21	0.06	−0.44	0.02
296	POR	cytochrome p450 oxidoreductase	Cytoplasm	0.41	0.00	−0.33	0.04
297	PPEF1	protein phosphatase with EF-hand domain 1	Extracellular Space	−0.22	0.00	0.23	0.02
298	PPP1R10	protein phosphatase 1 regulatory subunit 10	Nucleus	0.26	0.00	−0.58	0.01
299	PPP1R3E	protein phosphatase 1 regulatory subunit 3E	Cytoplasm	−0.28	0.04	−0.30	0.09
300	PPP1R9B	protein phosphatase 1 regulatory subunit 9B	Cytoplasm	−0.34	0.00	−0.26	0.04
301	PRELP	proline and arginine rich end leucine rich repeat protein	Extracellular Space	0.35	0.00	−0.25	0.07
302	Prrxl1	paired related homeobox protein-like 1	Other	0.24	0.00	−0.29	0.06
303	PRTN3	proteinase 3	Extracellular Space	0.58	0.01	−0.45	0.09
304	PSMA5	proteasome subunit alpha 5	Cytoplasm	−0.22	0.00	0.21	0.05
305	PSMB10	proteasome subunit beta 10	Cytoplasm	−0.22	0.08	0.29	0.10
306	PSMB3	proteasome subunit beta 3	Cytoplasm	−0.22	0.00	0.22	0.03
307	PSMB7	proteasome subunit beta 7	Cytoplasm	−0.21	0.00	0.20	0.05
308	PTPRU	protein tyrosine phosphatase receptor type U	Plasma Membrane	0.37	0.00	−0.32	0.04
309	PXN	paxillin	Cytoplasm	0.25	0.01	−0.25	0.08
310	RAB4A	RAB4A, member RAS oncogene family	Cytoplasm	0.24	0.00	−0.25	0.04
311	RASL10B	RAS like family 10 member B	Other	−0.21	0.00	−0.28	0.05
312	RAVER1	ribonucleoprotein, PTB binding 1	Nucleus	0.22	0.03	−0.48	0.01
313	RBM38	RNA binding motif protein 38	Nucleus	0.85	0.00	−0.57	0.02
314	RCC2	regulator of chromosome condensation 2	Nucleus	−0.21	0.00	−0.26	0.07
315	RCSD1	RCSD domain containing 1	Other	0.22	0.02	−0.23	0.06
316	REEP4	receptor accessory protein 4	Cytoplasm	0.33	0.01	−0.27	0.06
317	REEP6	receptor accessory protein 6	Plasma Membrane	0.38	0.04	−0.41	0.07
318	RELN	reelin	Extracellular Space	0.28	0.00	−0.38	0.03
319	Retnlg	resistin like gamma		0.49	0.07	−0.34	0.08

(*continued on next page*)

Table 1 (*continued*)

	Symbol	Entrez Gene Name	Location	PBS vs Cis		Cis vs Cis + TTI-101	
				log_2 Fold Change	Expr p-value	log_2 Fold Change	Expr p-value
			Extracellular Space				
320	RFXANK	regulatory factor X associated ankyrin containing protein	Nucleus	0.20	0.09	−0.21	0.08
321	RHCE/RHD	Rh blood group D antigen	Plasma Membrane	1.07	0.02	−0.54	0.05
322	RHOT2	ras homolog family member T2	Cytoplasm	0.20	0.00	−0.21	0.05
323	Rn18s-rs5	18 s RNA, related sequence 5	Other	−0.98	0.00	0.79	0.06
324	RNF123	ring finger protein 123	Cytoplasm	0.32	0.00	−0.27	0.09
325	RNF208	ring finger protein 208	Other	−0.22	0.02	−0.35	0.02
326	RNF216	ring finger protein 216	Cytoplasm	0.33	0.00	−0.36	0.08
327	RPAP1	RNA polymerase II associated protein 1	Other	0.33	0.00	−0.34	0.03
328	RPH3A	rabphilin 3A	Plasma Membrane	0.21	0.01	−0.50	0.01
329	Rpl22l1	ribosomal protein L22 like 1	Other	−0.27	0.00	0.20	0.06
330	RPL26	ribosomal protein L26	Cytoplasm	−0.21	0.00	0.22	0.04
331	RPL37A	ribosomal protein L37a	Cytoplasm	−0.21	0.00	0.22	0.04
332	RPS6KA1	ribosomal protein S6 kinase A1	Cytoplasm	0.32	0.00	−0.42	0.01
333	RRM2	ribonucleotide reductase regulatory subunit M2	Nucleus	0.91	0.00	−0.44	0.03
334	RTN4R	reticulon 4 receptor	Plasma Membrane	−0.22	0.08	−0.26	0.07
335	RXRG	retinoid X receptor gamma	Nucleus	0.28	0.00	−0.21	0.08
336	SAMD14	sterile alpha motif domain containing 14	Other	−0.21	0.01	−0.28	0.03
337	SAP130	Sin3A associated protein 130	Nucleus	0.42	0.00	−0.24	0.09
338	SCG2	secretogranin II	Extracellular Space	−0.22	0.01	0.20	0.08
339	SCN5A	sodium voltage-gated channel alpha subunit 5	Plasma Membrane	0.23	0.05	−0.31	0.05
340	SCRT1	scratch family transcriptional repressor 1	Nucleus	−0.23	0.04	−0.41	0.02
341	SCUBE1	signal peptide, CUB domain and EGF like domain containing 1	Plasma Membrane	0.26	0.01	−0.48	0.02
342	SDC3	syndecan 3	Plasma Membrane	−0.22	0.00	−0.25	0.07
343	SEC24C	SEC24 homolog C, COPII coat complex component	Cytoplasm	0.20	0.00	−0.29	0.03
344	SEMA4B	semaphorin 4B	Plasma Membrane	0.28	0.00	−0.23	0.07
345	SEMA4G	semaphorin 4G	Plasma Membrane	0.32	0.01	−0.47	0.00
346	SEPTIN8	septin 8	Extracellular Space	0.21	0.00	−0.23	0.05
347	SERPINA3	serpin family A member 3	Extracellular Space	−0.30	0.00	0.23	0.01
348	Serpina3g (includes others)	serine (or cysteine) peptidase inhibitor, clade A, member 3G	Cytoplasm	−0.49	0.01	0.22	0.03
349	SERPINB1	serpin family B member 1	Cytoplasm	−0.36	0.00	0.21	0.07
350	Serpinb1b	serine (or cysteine) peptidase inhibitor, clade B, member 1b	Other	−0.23	0.01	0.22	0.08
351	SEZ6L	seizure related 6 homolog like	Plasma Membrane	0.41	0.00	−0.59	0.01
352	SFRP5	secreted frizzled related protein 5	Plasma Membrane	−0.21	0.00	−0.30	0.00
353	SH2D3C	SH2 domain containing 3C	Cytoplasm	0.23	0.00	−0.24	0.10
354	SHMT2	serine hydroxymethyltransferase 2	Cytoplasm	0.23	0.02	−0.27	0.05
355	SIX5	SIX homeobox 5	Nucleus	0.32	0.09	−0.34	0.09
356	SKIV2L	Ski2 like RNA helicase	Nucleus	0.21	0.00	−0.32	0.03
357	SLC16A10	solute carrier family 16 member 10	Plasma Membrane	0.51	0.03	−0.45	0.05
358	SLC25A37	solute carrier family 25 member 37	Cytoplasm	0.64	0.00	−0.24	0.08
359	SLC40A1	solute carrier family 40 member 1	Plasma Membrane	0.56	0.00	−0.33	0.06
360	SLC4A11	solute carrier family 4 member 11	Plasma Membrane	0.29	0.00	−0.28	0.04
361	SLC7A8	solute carrier family 7 member 8	Plasma Membrane	0.48	0.00	−0.36	0.07
362	SLC9A1	solute carrier family 9 member A1	Plasma Membrane	0.23	0.01	−0.42	0.04
363	SLIT1	slit guidance ligand 1	Extracellular Space	0.24	0.01	−0.36	0.06
364	SLX4	SLX4 structure-specific endonuclease subunit	Nucleus	0.39	0.00	−0.24	0.06
365	SMTN	smoothelin	Extracellular Space	0.49	0.00	−0.37	0.03
366	SNCB	synuclein beta	Cytoplasm	−0.32	0.00	−0.25	0.06
367	SNPH	syntaphilin	Plasma Membrane	0.22	0.00	−0.31	0.02
368	SOBP	sine oculis binding protein homolog	Nucleus	−0.23	0.01	−0.34	0.02

(*continued on next page*)

Table 1 (*continued*)

	Symbol	Entrez Gene Name	Location	PBS vs Cis		Cis vs Cis + TTI-101	
				log_2 Fold Change	Expr p-value	log_2 Fold Change	Expr p-value
369	SOD3	superoxide dismutase 3	Extracellular Space	0.41	0.00	−0.49	0.02
370	SOX6	SRY-box transcription factor 6	Nucleus	0.24	0.04	−0.30	0.04
371	Spaca6	sperm acrosome associated 6	Other	0.42	0.02	0.33	0.04
372	SPECC1	sperm antigen with calponin homology and coiled-coil domains 1	Nucleus	0.22	0.05	−0.26	0.07
373	SPIRE2	spire type actin nucleation factor 2	Cytoplasm	−0.31	0.00	−0.27	0.02
374	SPSB3	splA/ryanodine receptor domain and SOCS box containing 3	Cytoplasm	0.23	0.06	−0.34	0.03
375	SPTBN5	spectrin beta, non-erythrocytic 5	Plasma Membrane	0.32	0.01	−0.36	0.05
376	SRCAP	Snf2 related CREBBP activator protein	Cytoplasm	0.20	0.10	−0.31	0.02
377	ST5	suppression of tumorigenicity 5	Cytoplasm	0.26	0.00	−0.25	0.09
378	STK10	serine/threonine kinase 10	Cytoplasm	0.21	0.03	−0.36	0.00
379	STUB1	STIP1 homology and U-box containing protein 1	Cytoplasm	0.24	0.00	−0.23	0.05
380	SUGP1	SURP and G-patch domain containing 1	Nucleus	0.32	0.00	−0.21	0.06
381	SYT2	synaptotagmin 2	Cytoplasm	0.24	0.01	−0.43	0.03
382	TAFA5	TAFA chemokine like family member 5	Extracellular Space	−0.25	0.00	−0.24	0.05
383	TBC1D17	TBC1 domain family member 17	Cytoplasm	0.24	0.00	−0.29	0.08
384	TCOF1	treacle ribosome biogenesis factor 1	Nucleus	0.23	0.07	−0.43	0.05
385	TECPR2	tectonin beta-propeller repeat containing 2	Other	0.20	0.01	−0.25	0.08
386	TENM2	teneurin transmembrane protein 2	Plasma Membrane	0.42	0.00	−0.28	0.08
387	TENM3	teneurin transmembrane protein 3	Plasma Membrane	0.26	0.00	−0.34	0.05
388	TENM4	teneurin transmembrane protein 4	Plasma Membrane	0.20	0.06	−0.46	0.02
389	TGFB1I1	transforming growth factor beta 1 induced transcript 1	Nucleus	0.35	0.00	−0.36	0.01
390	THBS1	thrombospondin 1	Extracellular Space	0.68	0.00	−0.24	0.02
391	THEM6	thioesterase superfamily member 6	Other	−0.23	0.00	−0.32	0.02
392	TIAM1	T cell lymphoma invasion and metastasis 1	Cytoplasm	0.30	0.00	−0.44	0.01
393	TINAGL1	tubulointerstitial nephritis antigen like 1	Extracellular Space	0.28	0.01	−0.35	0.03
394	TLN1	talin 1	Plasma Membrane	0.39	0.00	−0.39	0.05
395	TMEM151B	transmembrane protein 151B	Other	−0.30	0.00	−0.27	0.07
396	TMEM160	transmembrane protein 160	Cytoplasm	−0.25	0.02	0.24	0.07
397	TMEM205	transmembrane protein 205	Cytoplasm	−0.26	0.00	0.23	0.08
398	TNFAIP2	TNF alpha induced protein 2	Extracellular Space	0.53	0.00	−0.42	0.06
399	TNFRSF1A	TNF receptor superfamily member 1A	Plasma Membrane	0.23	0.01	−0.29	0.08
400	TNIP1	TNFAIP3 interacting protein 1	Nucleus	0.21	0.02	−0.38	0.01
401	TNXB	tenascin XB	Extracellular Space	0.26	0.01	−0.27	0.02
402	TOM1L2	target of myb1 like 2 membrane trafficking protein	Cytoplasm	0.21	0.00	−0.29	0.05
403	TONSL	tonsoku like, DNA repair protein	Cytoplasm	0.43	0.00	−0.38	0.05
404	TPRA1	transmembrane protein adipocyte associated 1	Plasma Membrane	0.28	0.00	−0.30	0.00
405	TPRN	taperin	Extracellular Space	−0.28	0.02	−0.26	0.08
406	TRPA1	transient receptor potential cation channel subfamily A member 1	Plasma Membrane	−0.31	0.00	0.29	0.02
407	TRPC6	transient receptor potential cation channel subfamily C member 6	Plasma Membrane	−0.20	0.04	0.29	0.01
408	TRPM2	transient receptor potential cation channel subfamily M member 2	Plasma Membrane	0.26	0.00	−0.23	0.05
409	TRRAP	transformation/transcription domain associated protein	Nucleus	0.37	0.00	−0.25	0.05
410	TSPAN18	tetraspanin 18	Other	0.25	0.00	−0.27	0.08
411	TSPAN33	tetraspanin 33	Plasma Membrane	0.46	0.02	−0.35	0.07
412	TTBK1	tau tubulin kinase 1	Other	−0.26	0.00	−0.40	0.02
413	TTC9B	tetratricopeptide repeat domain 9B	Other	−0.38	0.00	−0.24	0.09
414	TTLL3	tubulin tyrosine ligase like 3	Extracellular Space	0.61	0.00	−0.36	0.04
415	TTYH3	tweety family member 3	Plasma Membrane	−0.21	0.02	−0.23	0.09
416	UBC	ubiquitin C	Cytoplasm	0.58	0.00	−0.40	0.05
417	UBE3B	ubiquitin protein ligase E3B	Extracellular Space	0.31	0.00	−0.38	0.05
418	UBL7	ubiquitin like 7	Other	0.22	0.02	−0.25	0.10
419	UFSP2	UFM1 specific peptidase 2	Other	−0.22	0.00	0.20	0.06

(*continued on next page*)

Table 1 (*continued*)

	Symbol	Entrez Gene Name	Location	PBS vs Cis		Cis vs Cis + TTI-101	
				log_2 Fold Change	Expr p-value	log_2 Fold Change	Expr p-value
420	ULK3	unc-51 like kinase 3	Cytoplasm	0.27	0.00	−0.22	0.05
421	UNC5A	unc-5 netrin receptor A	Plasma Membrane	−0.27	0.05	−0.33	0.07
422	USP10	ubiquitin specific peptidase 10	Cytoplasm	0.31	0.00	−0.30	0.08
423	USP19	ubiquitin specific peptidase 19	Cytoplasm	0.20	0.01	−0.24	0.06
424	VGF	VGF nerve growth factor inducible	Extracellular Space	−0.73	0.00	−0.35	0.07
425	VPS18	VPS18 core subunit of CORVET and HOPS complexes	Cytoplasm	0.22	0.02	−0.35	0.05
426	VPS9D1	VPS9 domain containing 1	Other	0.22	0.01	−0.29	0.05
427	VWA5A	von Willebrand factor A domain containing 5A	Nucleus	−0.28	0.00	0.24	0.02
428	WASF1	WASP family member 1	Nucleus	−0.27	0.02	−0.29	0.06
429	WBP2	WW domain binding protein 2	Cytoplasm	0.28	0.00	−0.36	0.04
430	WDFY3	WD repeat and FYVE domain containing 3	Cytoplasm	0.22	0.01	−0.37	0.03
431	YLPM1	YLP motif containing 1	Nucleus	0.25	0.00	−0.24	0.02
432	ZDHHC18	zinc finger DHHC-type containing 18	Cytoplasm	−0.23	0.01	−0.29	0.05
433	ZFP36L1	ZFP36 ring finger protein like 1	Nucleus	0.23	0.03	−0.25	0.10
434	Zfp651	zinc finger protein 651	Other	−0.23	0.00	−0.21	0.03
435	ZFYVE26	zinc finger FYVE-type containing 26	Cytoplasm	0.44	0.00	−0.28	0.05
436	ZNF142	zinc finger protein 142	Nucleus	0.30	0.00	−0.23	0.09
437	ZNF219	zinc finger protein 219	Nucleus	−0.21	0.01	−0.28	0.02
438	ZNF423	zinc finger protein 423	Nucleus	0.26	0.01	−0.46	0.01
439	ZNF442	zinc finger protein 442	Nucleus	−0.22	0.05	0.35	0.09
440	ZNF592	zinc finger protein 592	Nucleus	0.27	0.01	−0.29	0.05
441	ZNF646	zinc finger protein 646	Nucleus	0.26	0.00	−0.26	0.04
442	ZNF703	zinc finger protein 703	Nucleus	−0.30	0.00	−0.27	0.07
443	ZSWIM1	zinc finger SWIM-type containing 1	Nucleus	0.35	0.00	−0.40	0.05

Table 2
Top five upstream regulators and their mechanistic network for differentially expressed.

	Upstream Regulator	Activation z-score	Overlap p-value	Mechanistic Network	Other Regulators in mechanistic network
1	HTT	−0.152	1.3E-10		
2	APP	2.394	1.67E-10	431 (8)	TP53, NOTCH1, SP1, TP73, HIF1A, MYC, **STAT3**
3	TP53	−2.078	1.77E-10	481 (14)	**STAT3**, ERBB2, TP73, HIF1A,SP1, ESTROGEN RECEPTOR, NOTCH1, CTNNB1, CREBBP ,SMAD4, SMAD3, FOS, STAT1
4	TGFB1	−5.111	2.84E-09	436 (13)	EGFP, ERBB2, NOTCH1, SP1, **STAT3**, EGR1, SMAD4, CREBBP, SMAD3, ESTROGEN RECEPTOR, CTNNB1, AR
5	estrogen receptor	−0.614	6.22E-09	558 (15)	TP53, BETA-ESTRADIOL, AR, CREBBP, ESR2, ESR1, SP1, TP73, HIF1A, **STAT3**, NOTCH1, DIETHYLSTILBESTEROL,4-HYDROXYTAMOXIFEN, ESTROGEN

genes in cisplatin dataset (cisplatin vs. cisplatin + TTI-101). Note, the number in the mechanistic network column denotes the number of target genes influenced by that particular regulator. The number in parenthesis denotes the total number of regulators in that mechanistic network.

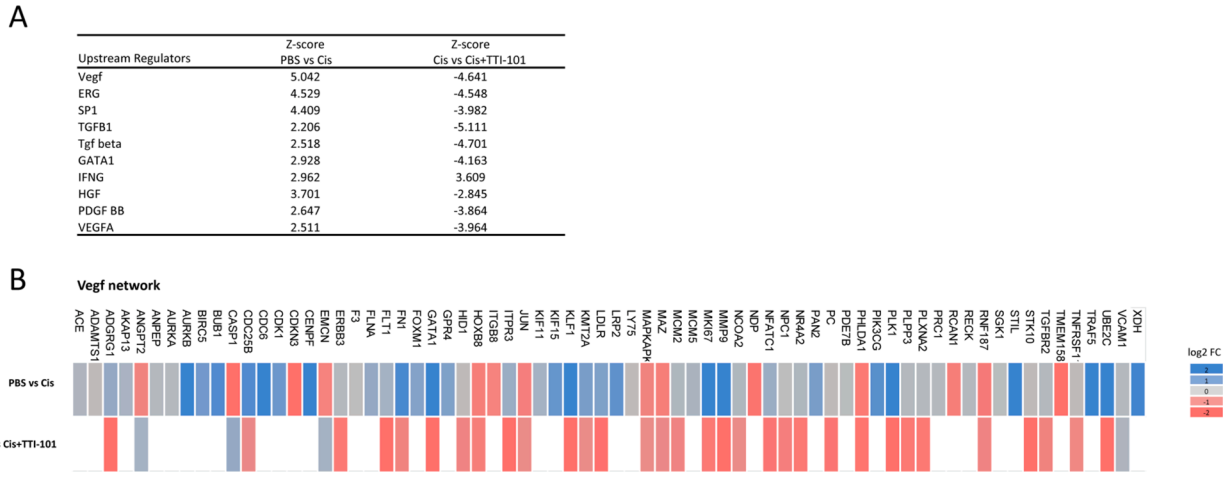

Fig. 9. Results of IPA comparison analyses. A. Top upstream regulators driving TTI-101-dependent changes in DRG identified using the IPA comparison analysis tool. IPA core analysis was performed between PBS vs. Cisplatin and Cisplatin vs. Cisplatin + TTI-101, followed by comparison of the two core analyses. B. Heat map showing details of target genes in VEGF network. Fold change data for target genes upregulated (blue) or downregulated (red) is shown.

It is conceivable that potential additional damage to mitochondria as a result of STAT3 inhibition would aggravate CIPN. However, our data demonstrated that TTI-101 treatment had the opposite effect; administration of TTI-101 suppressed established mechanical allodynia in mice treated with cisplatin. Preliminary data also indicated that TTI-101 suppressed existing mechanical allodynia in mice treated with paclitaxel or docetaxel, two chemotherapeutics of a different class. In addition, TTI-101 markedly reduced mechanical allodynia in the SNI model. SNI increases levels of pY-STAT3 in spinal cord astrocytes [34]. In addition, there is evidence for increased pY-STAT3 in microglia in the spinal cord in the spinal nerve injury model of neuropathic pain in rats [35]. While intrathecal administration of the Janus kinase 2 inhibitor, AG490, attenuated mechanical allodynia in both models [36], there are no published reports describing the effects of a STAT3 inhibitor on mechanical allodynia in response to SNI. Transgenic expression of constitutively active and dominant-negative forms of STAT3 in astrocytes located within the spinal dorsal horn (SDH) of mice and rats showed that activation of astrocytic STAT3 plays an important role in maintaining neuropathic pain [37]. Two previous studies reported the beneficial effect of STAT3 inhibitor treatment on chemotherapy-induced neuropathy; administration of the STAT3 inhibitor S3I-201 to rats during treatment with oxaliplatin, paclitaxel, or vincristine reduced mechanical allodynia [38,39]. However, the reduction in mechanical allodynia was only partial, and S3I-201 was administered intrathecally. Our data indicate that mechanical allodynia is reduced to baseline levels in response to oral administration of TTI-101, making this a more attractive compound for clinical application. It remains to be determined whether co-administration of TTI-101 with cisplatin will fully or partially prevent development of CIPN.

The beneficial effect of the STAT3 inhibitor S3I-201 in CIPN cited above was associated with normalization of the expression of CXCL12 a chemokine that was shown to be upregulated in the DRG of rats or mice treated with oxaliplatin, vincristine or paclitaxel. In our RNA-seq data set, we did not detect significant changes in CXCL12, although there was a trend towards increased levels (log2FC 0.176) in response to cisplatin and a trend towards reduced levels (log2FC −0.474) in response to administration of TTI-101 in cisplatin-treated mice. In addition, our RNA-seq analysis of the DRG transcriptome indicated that TTI-101 administration to cisplatin-treated mice normalizes expression of 443 out of the 1,973 genes (22 %) that were changed in response to cisplatin treatment. These genes are mainly associated with neuronal health and survival pathways, indicating that TTI-101 also may help to restore the loss in intra-epidermal nerve fiber density that is associated with CIPN. We also saw enrichment in genes related to the TNFR1 pathway after TTI-101 administration. This may indicate inhibition of TNF signaling, which has been shown to reduce STAT3 activation. In oxaliplatin-mediated neuropathy, administration of a neutralizing antibody against TNF-α prevented STAT3 activation in DRG [38].

To get additional insight into the potential mechanism underlying the suppression of cisplatin-induced mechanical allodynia, we used the IPA comparison analysis tool to identify upstream regulators of the pathways that were altered in response to cisplatin and reversed by administration of TTI-101. The STAT3 target VEGF [40,41] was identified as the top upstream regulator. It has been shown that activation of retinal neuronal STAT3 increases neuronal VEGF production [42]. In addition, DRG expression of *Flt1*, the gene encoding the VEGF receptor 1 (VEGF-R1), was upregulated in response to cisplatin (log2FC 0.295) and this was reversed by administration of TTI-101 (log2FC −0.503). We also found the VEGF-associated downstream kinase, PI3K, was downregulated by TTI-101 (log2FC −0.408). Interestingly, it has been shown that VEGF signaling to VEGFR1 on sensory neurons promotes pain in models of cancer pain [43]. Moreover, administration of an anti-VEGF antibody attenuated oxaliplatin-induced mechanical allodynia [44]. In addition, treatment with a PI3K inhibitor attenuated mechanical allodynia induced by VEGFA in mice. In contrast, however, there also is evidence for aggravation of chemotherapy-induced neuropathies by co-administration of anti-VEGF antibodies in patients and mice [45,46]. Further studies are needed to address the potential role of changes in local VEGF signaling in the DRG in the beneficial effect of TTI-101 on cisplatin-induced peripheral neuropathy.

We previously demonstrated that mitochondrial damage contributes to neuropathic pain [17,29]. STAT3 signaling is essential for mitochondrial function; consequently, reports of peripheral neuropathy as an SAE in clinical trials of STAT3 inhibitors that impair mitochondrial function were not totally unexpected. Here, we show that TTI-101, a competitive inhibitor STAT3, did not affect mitochondrial function and not only did not cause peripheral neuropathy, rather, it markedly reduced cisplatin-induced mechanical allodynia through modulating several signaling networks linked to CIPN. Thus, TTI-101 may be an attractive agent for cancer treatment, especially in combination with chemotherapy agents that cause CIPN.

Declaration of Competing Interest

Baylor College of Medicine, with David Tweardy as inventor, has filed 8 patent families covering the use of TTI-101, a small-molecule inhibitor of STAT3 used in this study. These patents are exclusively licensed to Tvardi Therapeutics, Inc., in which David Tweardy owns stock.

Acknowledgments

We thank the Mouse Metabolism and Phenotyping Core Facility at Baylor college of Medicine and the UT MD Anderson Proteomics and Metabolomics Facility, which is generously supported by the MD Anderson Cancer Center NIH High-End Instrumentation program grant 1S10OD012304-01 and CPRIT Core Facility Grant RP130397. These studies also were supported by NIH grants RO1DK114356 and UM1HG006348 and endowment funds from the University of Texas MD Anderson Cancer Center.

References

[1] U. Bharadwaj, M.M. Kasembeli, P. Robinson, D.J. Tweardy, Targeting janus kinases and signal transducer and activator of transcription 3 to treat inflammation, fibrosis, and cancer: rationale, progress, and caution, Pharmacol. Rev. 72 (2) (2020) 486–526.

[2] M. Kasembeli, U. Bharadwaj, P. Robinson, D. Tweardy, Contribution of STAT3 to inflammatory and fibrotic diseases and prospects for its targeting for treatment, Int. J. Mol. Sci. 19 (8) (2018) 2299, https://doi.org/10.3390/ijms19082299.

[3] C.V. Dang, E.P. Reddy, K.M. Shokat, L. Soucek, Drugging the 'undruggable' cancer targets, Nat. Rev. Cancer 17 (8) (2017) 502–508.

[4] J.C. Bendell, D.S. Hong, H.A. Burris, A. Naing, S.F. Jones, G. Falchook, P. Bricmont, A. Elekes, E.P. Rock, R. Kurzrock, Phase 1, open-label, dose-escalation, and pharmacokinetic study of STAT3 inhibitor OPB-31121 in subjects with advanced solid tumors, Cancer Chemother. Pharmacol. 74 (1) (2014) 125–130.

[5] M. Ogura, T. Uchida, Y. Terui, F. Hayakawa, Y. Kobayashi, M. Taniwaki, Y. Takamatsu, T. Naoe, K. Tobinai, W. Munakata, T. Yamauchi, A. Kageyama, M. Yuasa, M. Motoyama, T. Tsunoda, K. Hatake, Phase I study of OPB-51602, an oral inhibitor of signal transducer and activator of transcription 3, in patients with relapsed/refractory hematological malignancies, Cancer Sci. 106 (7) (2015) 896–901.

[6] D. Genini, L. Brambilla, E. Laurini, J. Merulla, G. Civenni, S. Pandit, R. D'Antuono, L. Perez, D.E. Levy, S. Pricl, G.M. Carbone, C.V. Catapano, Mitochondrial dysfunction induced by a SH2 domain-targeting STAT3 inhibitor leads to metabolic synthetic lethality in cancer cells, PNAS 114 (25) (2017) E4924–E4933.

[7] D.J. Garama, T.J. Harris, C.L. White, F.J. Rossello, M. Abdul-Hay, D.J. Gough, D. E. Levy, A Synthetic Lethal Interaction between Glutathione Synthesis and Mitochondrial Reactive Oxygen Species Provides a Tumor-Specific Vulnerability Dependent on STAT3, Mol. Cell. Biol. 35 (21) (2015) 3646–3656.

[8] R. Yang, M. Rincon, Mitochondrial Stat3, the Need for Design Thinking, International journal of biological sciences 12 (5) (2016) 532–544.

[9] U. Bharadwaj, T.K. Eckols, X. Xu, M.M. Kasembeli, Y. Chen, M. Adachi, Y. Song, Q. Mo, S.Y. Lai, D.J. Tweardy, Small-molecule inhibition of STAT3 in radioresistant head and neck squamous cell carcinoma, Oncotarget 7 (18) (2016) 26307–26330.

[10] U. Bharadwaj, M.M. Kasembeli, D.J. Tweardy, STAT3 Inhibitors in Cancer: A Comprehensive Update, in: A.C. Ward (Ed.), STAT Inhibitors in Cancer, Springer International Publishing, Cham, 2016, pp. 95–161.

[11] NCT03195699, Oral STAT3 Inhibitor, TTI-101, in Patients With Advanced Cancers, June 22, 2017. https://ClinicalTrials.gov/show/NCT03195699.

[12] S. Tyanova, T. Temu, J. Cox, The MaxQuant computational platform for mass spectrometry-based shotgun proteomics, Nat. Protoc. 11 (12) (2016) 2301–2319.
[13] P. Antinori, T. Michelot, P. Lescuyer, M. Müller, A.E. Acosta-Martin, Detection of Unknown Chemical Adduct Modifications on Proteins: From Wet to Dry Laboratory, in: C.A. Evans, P.C. Wright, J. Noirel (Eds.), Mass Spectrometry of Proteins: Methods and Protocols, Springer, New York, NY, 2019, pp. 99–113.
[14] M. Zimmermann, Ethical guidelines for investigations of experimental pain in conscious animals, Pain 16 (2) (1983) 109–110.
[15] C. Kilkenny, W.J. Browne, I.C. Cuthill, M. Emerson, D.G. Altman, Improving bioscience research reporting: the ARRIVE guidelines for reporting animal research, PLoS Biol. 8 (6) (2010) e1000412.
[16] S.R. Chaplan, F.W. Bach, J.W. Pogrel, J.M. Chung, T.L. Yaksh, Quantitative assessment of tactile allodynia in the rat paw, J. Neurosci. Methods 53 (1) (1994) 55–63.
[17] K. Krukowski, J. Ma, O. Golonzhka, G.O. Laumet, T. Gutti, J.H. van Duzer, R. Mazitschek, M.B. Jarpe, C.J. Heijnen, A. Kavelaars, HDAC6 inhibition effectively reverses chemotherapy-induced peripheral neuropathy, Pain 158 (6) (2017) 1126–1137.
[18] Q.-L. Mao-Ying, A. Kavelaars, K. Krukowski, X.-J. Huo, W. Zhou, T.J. Price, C. Cleeland, C.J. Heijnen, D.D. McKemy, The anti-diabetic drug metformin protects against chemotherapy-induced peripheral neuropathy in a mouse model, PLoS ONE 9 (6) (2014) e100701.
[19] P. Singhmar, R.T.P. Trinh, J. Ma, XiaoJiao Huo, B.o. Peng, C.J. Heijnen, A. Kavelaars, The fibroblast-derived protein PI16 controls neuropathic pain, PNAS 117 (10) (2020) 5463–5471.
[20] G.S. Chiu, N. Boukelmoune, A.C.A. Chiang, B.o. Peng, V. Rao, C. Kingsley, H.-L. Liu, A. Kavelaars, S.R. Kesler, C.J. Heijnen, Nasal administration of mesenchymal stem cells restores cisplatin-induced cognitive impairment and brain damage in mice, Oncotarget 9 (85) (2018) 35581–35597.
[21] J. Ma, R.T. Trinh, I.D. Mahant, B.o. Peng, P. Matthias, C.J. Heijnen, A. Kavelaars, Cell-specific role of histone deacetylase 6 in chemotherapy-induced mechanical allodynia and loss of intraepidermal nerve fibers, Pain 160 (12) (2019) 2877–2890.
[22] J.A. Dykens, Y. Will, The significance of mitochondrial toxicity testing in drug development, Drug Discovery Today 12 (17-18) (2007) 777–785.
[23] N. Amireddy, S.N. Puttapaka, R.L. Vinnakota, H.G. Ravuri, S. Thonda, S. V. Kalivendi, The unintended mitochondrial uncoupling effects of the FDA-approved anti-helminth drug nitazoxanide mitigates experimental parkinsonism in mice, J. Biol. Chem. 292 (38) (2017) 15731–15743.
[24] M.D. Brand, D.G. Nicholls, Assessing mitochondrial dysfunction in cells, Biochem. J. 435 (2) (2011) 297–312.
[25] X. Xu, M.M. Kasembeli, X. Jiang, B.J. Tweardy, D.J. Tweardy, H.H.H.W. Schmidt, Chemical probes that competitively and selectively inhibit Stat3 activation, PLoS ONE 4 (3) (2009) e4783.
[26] J.A. Ward, A. Pinto-Fernandez, L. Cornelissen, S. Bonham, L. Diaz-Saez, O. Riant, K.V.M. Huber, B.M. Kessler, O. Feron, E.W. Tate, Re-evaluating the mechanism of action of alpha, beta-unsaturated carbonyl DUB inhibitors b-AP15 and VLX1570: A paradigmatic example of unspecific protein cross-linking with michael acceptor motif-containing drugs, J. Med. Chem. (2020).
[27] J.S. McMurray, A new small-molecule Stat3 inhibitor, Chem. Biol. 13 (11) (2006) 1123–1124.
[28] D.P. Ball, A.M. Lewis, D. Williams, D. Resetca, D.J. Wilson, P.T. Gunning, Signal transducer and activator of transcription 3 (STAT3) inhibitor, S3I–201, acts as a potent and non-selective alkylating agent, Oncotarget 7 (15) (2016) 20669–20679.
[29] M.A. Maj, J. Ma, K.N. Krukowski, A. Kavelaars, C.J. Heijnen, Inhibition of mitochondrial p53 accumulation by PFT-μ prevents cisplatin-induced peripheral neuropathy, Front. Mol. Neurosci. 10 (2017) 108.
[30] H. Song, R. Wang, S. Wang, J. Lin, A low-molecular-weight compound discovered through virtual database screening inhibits Stat3 function in breast cancer cells, Proceedings of the National Academy of Sciences of the United States of America 102(13) (2005) 4700.
[31] G.J. Bennett, T. Doyle, D. Salvemini, Mitotoxicity in distal symmetrical sensory peripheral neuropathies. Nature reviews, Neurology 10 (6) (2014) 326–336.
[32] L.A. Colvin, Chemotherapy-induced peripheral neuropathy: where are we now? Pain 160 Suppl 1 (Suppl 1) (2019) S1–S10.
[33] J. Ma, A. Kavelaars, P.M. Dougherty, C.J. Heijnen, Beyond symptomatic relief for chemotherapy-induced peripheral neuropathy: Targeting the source, Cancer 124 (11) (2018) 2289–2298.
[34] S. Liu, W.L. Mi, Q. Li, M.T. Zhang, P. Han, S. Hu, Q.L. Mao-Ying, Y.Q. Wang, Spinal IL-33/ST2 Signaling Contributes to Neuropathic Pain via Neuronal CaMKII-CREB and Astroglial JAK2-STAT3 Cascades in Mice, Anesthesiology 123 (5) (2015) 1154–1169.
[35] E. Dominguez, C. Rivat, B. Pommier, A. Mauborgne, M. Pohl, JAK/STAT3 pathway is activated in spinal cord microglia after peripheral nerve injury and contributes to neuropathic pain development in rat, J. Neurochem. 107 (1) (2008) 50–60.
[36] M. Tsuda, Y. Kohro, T. Yano, T. Tsujikawa, J. Kitano, H. Tozaki-Saitoh, S. Koyanagi, S. Ohdo, R.R. Ji, M.W. Salter, K. Inoue, JAK-STAT3 pathway regulates spinal astrocyte proliferation and neuropathic pain maintenance in rats, Brain 134 (Pt 4) (2011) 1127–1139.
[37] Y. Kohro, E. Sakaguchi, R. Tashima, H. Tozaki-Saitoh, H. Okano, K. Inoue, M. Tsuda, A new minimally-invasive method for microinjection into the mouse spinal dorsal horn, Sci. Rep. 5 (2015) 14306.
[38] Y.Y. Li, H. Li, Z.L. Liu, Q. Li, H.W. Qiu, L.J. Zeng, W. Yang, X.Z. Zhang, Z.Y. Li, Activation of STAT3-mediated CXCL12 up-regulation in the dorsal root ganglion contributes to oxaliplatin-induced chronic pain, Molecular pain 13 (2017) 1744806917747425.
[39] T. Xu, X.-L. Zhang, H.-D. Ou-Yang, Z.-Y. Li, C.-C. Liu, Z.-Z. Huang, J. Xu, J.-Y. Wei, B.-L. Nie, C. Ma, S.-L. Wu, W.-J. Xin, Epigenetic upregulation of CXCL12 expression mediates antitubulin chemotherapeutics-induced neuropathic pain, Pain 158 (4) (2017) 637–648.
[40] D. Wei, X. Le, L. Zheng, L. Wang, J.A. Frey, A.C. Gao, Z. Peng, S. Huang, H. Q. Xiong, J.L. Abbruzzese, K. Xie, Stat3 activation regulates the expression of vascular endothelial growth factor and human pancreatic cancer angiogenesis and metastasis, Oncogene 22 (3) (2003) 319–329.
[41] G. Niu, K.L. Wright, M. Huang, L. Song, E. Haura, J. Turkson, S. Zhang, T. Wang, D. Sinibaldi, D. Coppola, R. Heller, L.M. Ellis, J. Karras, J. Bromberg, D. Pardoll, R. Jove, H. Yu, Constitutive Stat3 activity up-regulates VEGF expression and tumor angiogenesis, Oncogene 21 (13) (2002) 2000–2008.
[42] Y. Sun, M. Ju, Z. Lin, T.W. Fredrick, L.P. Evans, K.T. Tian, N.J. Saba, P.C. Morss, W. T. Pu, J. Chen, A. Stahl, J.S. Joyal, L.E. Smith, SOCS3 in retinal neurons and glial cells suppresses VEGF signaling to prevent pathological neovascular growth, Science signaling 8(395) (2015) ra94.
[43] D. Selvaraj, V. Gangadharan, C. Michalski, M. Kurejova, S. Stösser, K. Srivastava, M. Schweizerhof, J. Waltenberger, N. Ferrara, P. Heppenstall, M. Shibuya, H. Augustin, R. Kuner, A functional role for VEGFR1 expressed in peripheral sensory neurons in cancer pain, Cancer Cell 27 (6) (2015) 780–796.
[44] L. Di Cesare Mannelli, B. Tenci, L. Micheli, A. Vona, F. Corti, M. Zanardelli, A. Lapucci, A.M. Clemente, P. Failli, C. Ghelardini, Adipose-derived stem cells decrease pain in a rat model of oxaliplatin-induced neuropathy: Role of VEGF-A modulation, Neuropharmacology 131 (2018) 166–175.
[45] B.J. Giantonio, P.J. Catalano, N.J. Meropol, P.J. O'Dwyer, E.P. Mitchell, S. R. Alberts, M.A. Schwartz, A.B. Benson 3rd, Bevacizumab in combination with oxaliplatin, fluorouracil, and leucovorin (FOLFOX4) for previously treated metastatic colorectal cancer: results from the Eastern Cooperative Oncology Group Study E3200, J. Clin. Oncol. 25 (12) (2007) 1539–1544.
[46] A. Verheyen, E. Peeraer, R. Nuydens, J. Dhondt, K. Poesen, I. Pintelon, A. Daniels, J.P. Timmermans, T. Meert, P. Carmeliet, D. Lambrechts, Systemic anti-vascular endothelial growth factor therapies induce a painful sensory neuropathy, Brain 135 (Pt 9) (2012) 2629–2641.
[47] D.R. Brademan, N.M. Riley, N.W. Kwiecien, J.J. Coon, Interactive peptide spectral annotator: A versatile web-based tool for proteomic applications, Mol. Cell. Proteom. MCP 18 (8) (2019) S193–S201.